nature cell biology

Spatial regulation of Fus3 MAP kinase activity through a reaction-diffusion mechanism in yeast pheromone signalling

Celine I. Maeder[1,4], Mark A. Hink[2,4], Ali Kinkhabwala[2], Reinhard Mayr[1,3], Philippe I. H. Bastiaens[2,5] and Michael Knop[1,5]

Signal transduction through mitogen-activated protein kinase (MAPK) cascades is thought to occur through the assembly of macromolecular complexes. We quantified the abundance of complexes in the cytoplasm among the MAPKs Ste11, Ste7, Fus3 and the scaffold protein Ste5 in yeast pheromone signalling using fluorescence cross-correlation spectroscopy (FCCS). Significant complex concentrations were observed that remained unchanged on pheromone stimulation, demonstrating that global changes in complex abundances do not contribute to the transmission of signal through the cytoplasm. On the other hand, investigation of the distribution of active Fus3 ($Fus3^{PP}$) across the cytoplasm using fluorescence lifetime imaging microscopy (FLIM) revealed a gradient of $Fus3^{PP}$ activity emanating from the tip of the mating projection. Spatial partitioning of Fus3 activating kinases to this site and deactivating phosphatases in the cytoplasm maintain this $Fus3^{PP}$-activity distribution. Propagation of signalling from the shmoo is, therefore, spatially constrained by a gradient-generating reaction-diffusion mechanism.

The response of the yeast *Saccharomyces cerevisiae* to mating pheromone is mediated by a canonical MAPK signalling cascade. Pheromone stimulation of a specific G-protein coupled receptor (GPCR) results in activation of the signalling cascade, as well as other signalling networks. These integrate cell-cycle regulation and coordinate cell polarity and exocytotic machinery to locally form a precisely oriented mating projection known as the shmoo[1]. The transcriptional response specifically leads to modulation of the expression of signalling molecules and to the production of molecules necessary for both cellular and subsequent nuclear fusion events.

The binding of pheromone at the GPCR activates a trimeric G-protein ($G_{\alpha\beta\gamma}$; also known as Gpa1, Ste4 and Ste18; Fig. 1a). The released $G_{\beta\gamma}$ dimer, which is attached to the membrane through a lipid anchor, interacts with the PAK kinase Ste20 and the scaffold protein Ste5. In conjunction with bound Ste4 (ref. 2), a conformational change of Ste5 is generated that results in Ste5 oligomerization and the activation of Ste11 (also known as MAPKKK) via Cdc42-activated Ste20. Requirements for Ste7 (also known as MAPKK) and Fus3 (also known as MAPK) phosphorylation include: the membrane recruitment of Ste5 through cryptic lipid-binding domains; the interaction of Ste5 with $G_{\beta\gamma}$; and the self-interaction of Ste5 (refs 3, 4). Fus3 phosphorylation of its Thr 180 and Tyr 182 residues in the activation loop generates the active form of Fus3, $Fus3^{PP}$. The high turnover rate of Fus3 at the tip of the mating projection may arise from displacement following phosphorylation by its activating kinase Ste7 (ref. 5). The nuclear pool of $Fus3^{PP}$ regulates a series of transcriptional regulators that modulate mating-specific gene expression[6].

It is currently unknown whether changes in complex formation among the scaffold protein Ste5 and the MAPKs Ste11, Ste7 and Fus3 account for signal transduction, and how this is spatially organized. We have addressed these questions of signal propagation through *in vivo* quantification of MAPK complexes, and by imaging the spatial distribution of $Fus3^{PP}$ activity in quiescent and signalling cells.

RESULTS

Pheromone stimulation does not change cytoplasmic MAPK complexes

Two different protein components of the MAPK-scaffold module were tagged with 3meGFP (tandem array of three monomeric yeast-enhanced GFPs) or 3mCherry (tandem array of three mCherry; see Supplementary Information), expressed at endogenous levels from their chromosomal locations. After establishing the functionality of these gene fusions (see Supplementary Information, Fig. S1), confocal microscopy imaging demonstrated that all proteins localized to the cytoplasm in vegetative

[1]Cell Biology and Biophysics Unit, EMBL-Heidelberg, Meyerhofstrasse 1, D-69117 Heidelberg, Germany. [2]Max Planck Institute for Molecular Physiology, Department of Systemic Cell Biology, Otto-Hahn-Str. 11, 44227 Dortmund, Germany. [3]Current address: Upper Austrian Research GmbH, Center for Biomedical Nanotechnology (CBN), Scharitzerstraße 6-8, 4020 Linz, Austria. [4]These authors contributed equally to this work.
[5]Correspondence should be addressed to M.K. or P.I.H.B. (email: knop@embl.de; bastiaens@mpi-dortmund.mpg.de)

Received 26 June 2007; accepted 30 August 2007; published online 21 October 2007; DOI: 10.1038/ncb1652

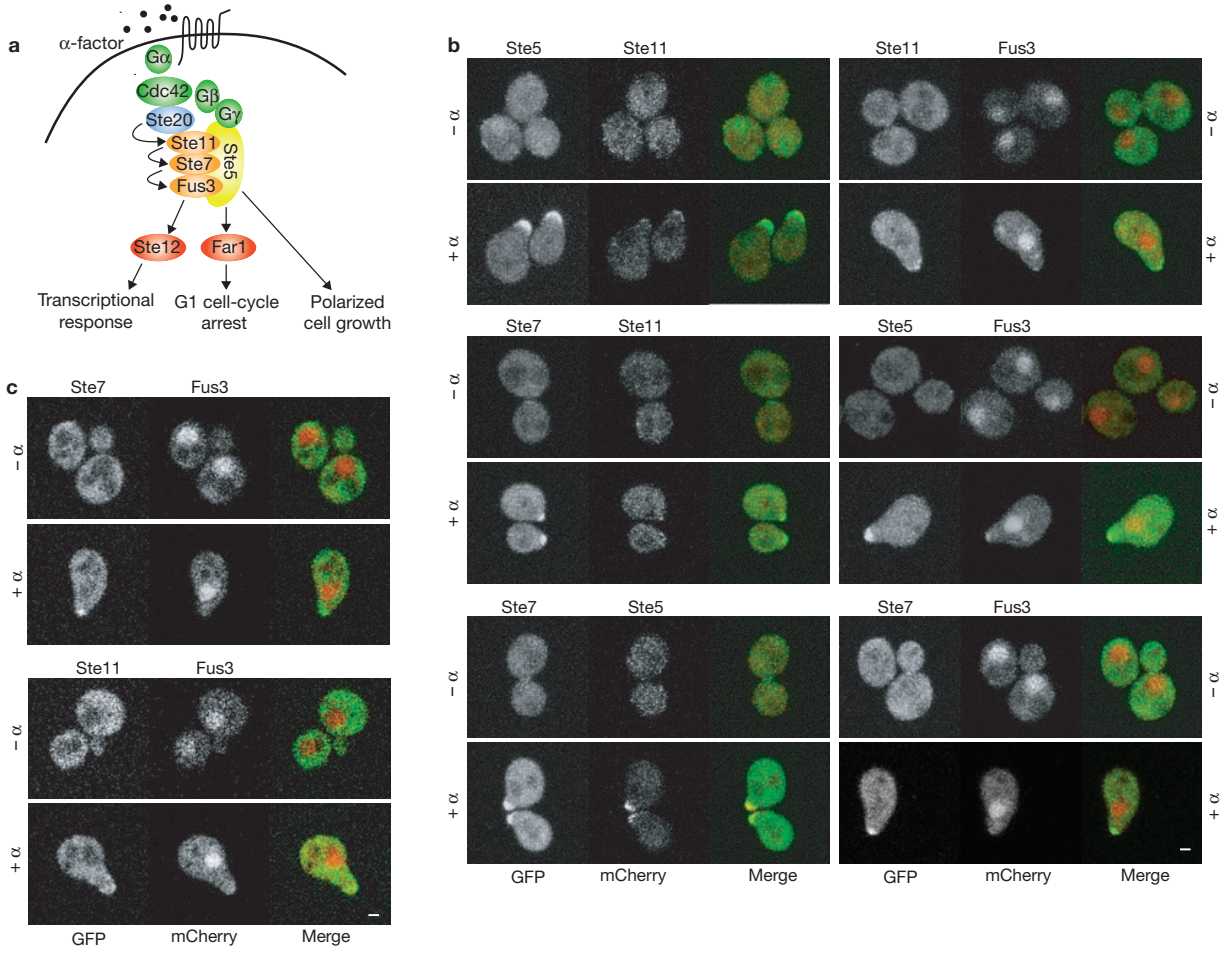

Figure 1 Localization of endogenously expressed Ste5, Ste7, Ste11 and Fus3 in vegetative and pheromone-stimulated cells. (**a**) Schematic representation of the MAPK module in yeast pheromone signaling (adapted from ref. 28). (**b**) Confocal microscopy images of fluorescent protein-tagged MAPK proteins before and 2.5–3 h after stimulation with 10 μg ml^{-1} α-factor. *z*-stacks were acquired and processed as described in the Methods. Maximum projections are shown. (**c**) Confocal microscopy cross-sections showing that Ste11 and Ste7 are excluded from the nucleus. The scale bars represent 1 μm in **b** and **c**.

cells (Fig. 1b). Ste5 was present at equal levels in the nucleus and cytoplasm, whereas Fus3 exhibited a three-fold accumulation in the nucleus compared to the cytoplasm, and Ste7 and Ste11 were predominantly cytoplasmic (Fig. 1c). Pheromone stimulation led to enrichment of Ste5, Ste7 and Fus3, but hardly any Ste11, at the shmoo tip (Fig. 1b).

Using fluorescence correlation spectroscopy (FCS; see Methods), the cytoplasmic concentrations of the individual protein components were obtained. Fus3 was the most abundant, with Ste5, Ste7 and Ste11 all present at levels roughly 15–30% of the Fus3 concentration (see Supplementary Information, Fig. S2). *In vivo* FCCS[7] (see Methods and Supplementary Information, Fig. S3) was established to quantify protein complexes in yeast. All six binary interactions between Ste5, Ste7, Ste11 and Fus3 were quantified in unbudded vegetative and in pheromone-stimulated cells. The measurements were taken during the first hour of stimulation, during which the peak of Fus3 activity is reached[8] without significant changes in the expression levels of the proteins comprising the MAPK module (Fig. 2). Any observed change in complex abundances will therefore be due to signalling activity (for example, affinity regulation by post-translational modifications) and not to mass action by changes in component concentrations. The complex between Ste7 and Fus3 was most abundant, with approximately half of Ste7 bound to Fus3 (Fig. 2). The amount of the other complexes was lower, in the range of 4–33% (expressed as a molar fraction of complex relative to the component with lower abundance). Effective dissociation constants (K_D^{eff}) were calculated for each interaction pair from the FCCS data (see Methods and Supplementary Information, Table S2 and Fig. S4). Comparison of vegetative cells with pheromone-stimulated cells revealed no significant changes for all K_D^{eff} values (Fig. 2), demonstrating that there are no changes in cytoplasmic complex formation among the MAPKs and the scaffold Ste5 induced by pheromone signalling.

Recruitment of MAPKs to the shmoo tip

It is unclear whether pheromone signalling involves change in complex formation between the components of the MAPK module. One possibility might be that shmoo-tip recruitment is accompanied by changes in protein-complex formation. We therefore quantified the relative abundance of shmoo-bound components using FCS-calibrated image analysis (see Supplementary Information, Fig. S5). Results for the MAPKs are shown as the relative molar abundances of each component versus Ste5 (Fig. 3a, b). The molar ratio of Ste11 to Ste5 was 0.2 at the shmoo tip

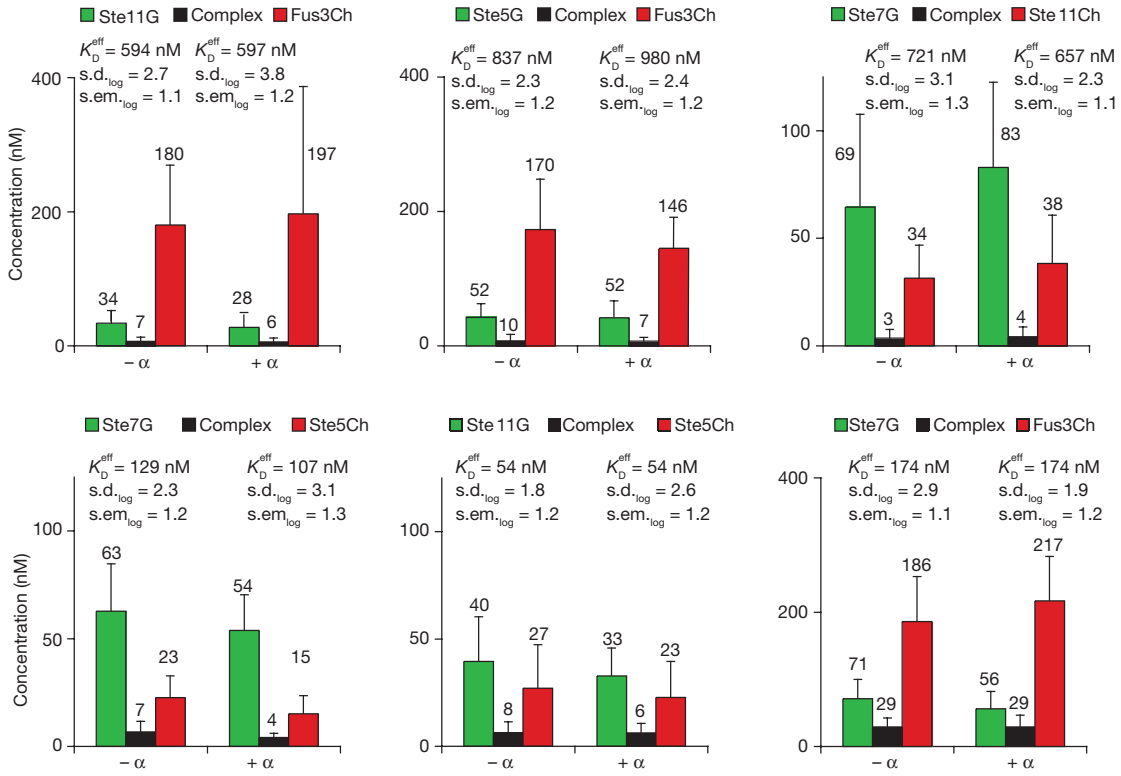

Figure 2 Quantification of complexes between Ste5, Ste7, Ste11 and Fus3 in the cytoplasm through measurement of all six pair-wise interactions. Protein and complex concentration were measured in the cytoplasm of untreated and stimulated cells (<1 h after addition of α-factor). Mean values (numbers above bars) and s.d. are given for measurements in 30–90 individual cells. Single-cell values for K_D^{eff} followed log-normal distributions. The mean K_D^{eff} was therefore calculated in log units. The population spread and s.e.m. were also calculated in log units and are labelled s.d.$_{log}$ and s.e.m.$_{log}$, respectively, which are scaling factors of the mean in normal units (see Methods). Ch, 3mCherry; G, 3meGFP.

and was, therefore, similar to that detected in the cytoplasm by FCCS (Fig. 3a, b). The same result was obtained in a strain with a reversed chromophore combination (data not shown). This result suggests that membrane recruitment has no effect on the Ste5–Ste11 complex.

The Ste7 concentration at the shmoo tip was roughly equivalent to Ste5 (Fig. 3b), in contrast with the much lower molar fraction of Ste5 bound to Ste7 in the cytoplasm (Fig. 3a). The Ste7–Ste5 interaction is not thought to depend on the activation of Ste5, or on signalling in general[9], indicating that the higher fraction at the shmoo tip may be due to Ste5-independent recruitment of Ste7 — for example, via the scaffolding molecule Spa2 (refs 10, 11).

Fus3 concentration at the shmoo tip exceeded Ste5 concentration approximately 1.7-fold (Fig. 3b). This may be explained by locally enriched substrates of Fus3 at the shmoo tip having docking sites[12] that can bind and retain active Fus3^{PP} via enzyme–substrate interactions. Futhermore, a series of studies report shmoo tip-localized substrates of Fus3, and evidence has been provided that active Fus3^{PP} can participate in relatively stable protein–protein interactions (see Supplementary Information).

To determine whether substrate interactions contribute to Fus3 recruitment in the shmoo, the shmoo-tip abundance of Fus3 mutants was quantitatively compared with wild-type Fus3 coexpressed in the same cells. Expression of the kinase-dead Fus3 (Fus3^{K42R}) led to a partial displacement of wild-type Fus3 from the shmoo (Fig. 3c), which may be caused by enhanced substrate binding. Such changes in the affinity to substrates have been reported for active site mutants of protein kinase A[13]. In contrast, a Fus3 mutant that is partially impaired in the canonical MAPK docking interactions (Fus3$^{D314K, D317K}$, Fus3^{DDKK}) was present in the shmoo at significantly lower levels, roughly 50% of the wild type. Fus3^{DDKK} was also impaired in binding to Ste7 in the cytoplasm, as determined by FCCS (Fig. 3d), which may contribute to the lower binding in the shmoo. The same level of reduction at the shmoo tip was also observed for a non-phosphorylatable Fus3 (Fus3$^{T180A, Y182F}$, Fus3^{TYAF}), which was not impaired in docking interactions to Ste7 in the cytoplasm (Fig. 3d). Crystallographic studies have provided no indication that phosphorylation of the activation loop leads to any conformational change of Fus3 (ref. 14) that could cause the enhanced affinity of the activated kinase to docking peptides. Therefore, the decreased shmoo localization of Fus3^{TYAF} is more likely due to impaired enzyme–substrate interactions mediated by the active site.

Ste5 mutants with impaired binding to Fus3 (Ste5ND; ref. 14) were shown to cause hyperactivation of pheromone signalling due to the requirement of the Ste5–Fus3 interaction for the formation of a specific pool of mono-phosphorylated Fus3^{P} (at Tyr 182), which acts through a feedback phosphorylation reaction on Ste5. This leads to downregulation of the signalling capacity[14]. Ste5ND did not affect the localization of Fus3 to the shmoo tip (Fig. 3e), despite its much-reduced interaction with the kinase (as confirmed by FCCS measurements in the cytoplasm; Fig. 3d). However, Ste5ND itself exhibited roughly 1.5-fold enrichment in the shmoo, indicating that Fus3-binding may regulate

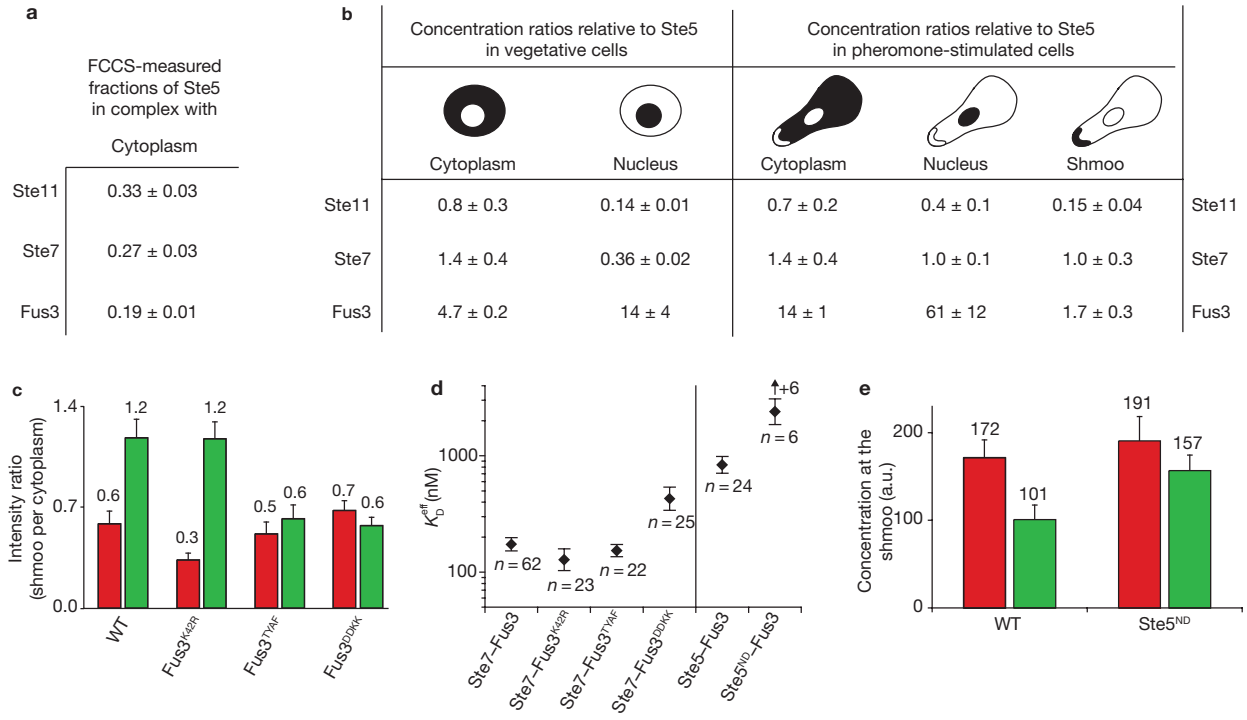

Figure 3 Recruitment of active Fus3^{PP} to the shmoo. (**a**) FCCS-measured fraction of Ste5 in complex with the different MAPKs. (**b**) Quantification of relative MAPK abundances at different sites in yeast cells using APD imaging and image analysis (see Methods). The relative abundance of the three kinases (Ste11, Ste7 and Fus3) versus the scaffold Ste5 in vegetative or pheromone stimulated cells is given at the cellular locations indicated in the schematic representations. Cells were stimulated with α-factor for 2.5–3 h. Error values indicate the s.e.m. Abundances at the shmoo tip were quantified in 20–60 cells. (**c**) Enrichment of Fus3 mutants in the shmoo. Enrichment of wild-type Fus3 (labelled with 3mCherry; red) and Fus3-mutant protein (labelled with 3meGFP; green) in the shmoo in stimulated cells (after 2.5–3 h stimulation). Wild-type Fus3 and mutant Fus3 were expressed in parallel in the same cells. Fus3^{K42R}, kinase dead; Fus3^{TYAF}, non-activatable; Fus3^{DDKK}, substrate docking-site mutant. (**d**) K_D^{eff} of complexes of Fus3 mutants with Ste7 and of the Ste5ND mutant with Fus3 in vegetative cells determined by FCCS. The K_D^{eff} values were calculated in logarithmic units (see Methods). The interaction of Fus3^{DDKK} with Ste7 was significantly weaker (statistical parameters, including *P* values for the comparison of the interactions in different strains, are shown in Supplementary Information, Table S2), but not completely abolished, as the mutations in Fus3 only partially affect the binding to docking peptides[12]. The interaction of Fus3^{DDKK} to Ste5 was not significantly affected (data not shown), probably due to the bipartite nature of this interaction[14]. The interaction of Ste5ND with Fus3 was significantly weaker (see Supplementary Information, Table S2), with no observable level of interaction detected in six cells (indicated by the arrow). These cells could not be used for the calculation of the K_D^{eff} (lower limit). (**e**) Enrichment of Fus3 (red) and Ste5 (green) in the shmoo of wild-type and Fus3-binding impaired Ste5ND cells after 2.5–3 h stimulation. Mean values and s.e.m. for 30–50 cells are shown.

the localization of Ste5 via phosphorylation[14], possibly through modulation of Ste5 oligomerization or Ste5 interaction with the membrane. Taken together, these results support the hypothesis that active Fus3^{PP} is bound to the shmoo via enzyme–substrate interactions.

Cytoplasmic phosphatase levels limit Fus3 enrichment in the shmoo

The enrichment of active Fus3^{PP} in the shmoo could be caused by locally enriched substrates and/or by the restriction of diffusible active Fus3^{PP} to the shmoo region. In the latter case, Fus3 must be activated locally at the shmoo and, through some counteracting mechanism, prevented from spreading across the cell cytoplasm. This could be mediated by phosphatases, in particular Msg5 and Ptp3, which are known to dephosphorylate active Fus3^{PP}. In fully stimulated cells, these phosphatases limit the amount of phosphorylated Fus3, indicating that a steady-state level of active Fus3^{PP} is maintained by a phosphorylation-dephosphorylation cycle[8,15,16]. These phosphatases were uniformly distributed in the cytoplasm with significantly lower concentration in the nucleus (Fig. 4a, b). On stimulation, Msg5, but not Ptp3 levels increased approximately two-fold (Fig. 4b). No accumulation of the phosphatases at the shmoo tip was observed.

Phosphatase levels determine the amount of active Fus3^{PP} in cells, therefore, alteration of these levels should also influence the abundance of Fus3 at the shmoo tip. This was indeed the case, as underexpression of Msg5 resulted in an increase in the abundance of Fus3 at the shmoo tip, whereas the opposite was true for moderate overexpression (Fig. 4c), confirming the role of phosphatases in maintaining active Fus3^{PP} at the shmoo tip.

A cytoplasmic gradient of active Fus3^{PP} emanating from the shmoo tip

The dynamic cycle of local Fus3 activation at the shmoo tip and uniform inactivation throughout the cytoplasm (by Ptp3 and Msg5) is capable of generating a gradient of active Fus3^{PP} emanating from the shmoo[17,18] that could localize Fus3^{PP} activity. A gradient with significant contrast, however, requires the inactivation timescale of Fus3^{PP} (via dephosphorylation) to be comparable or faster than the diffusion

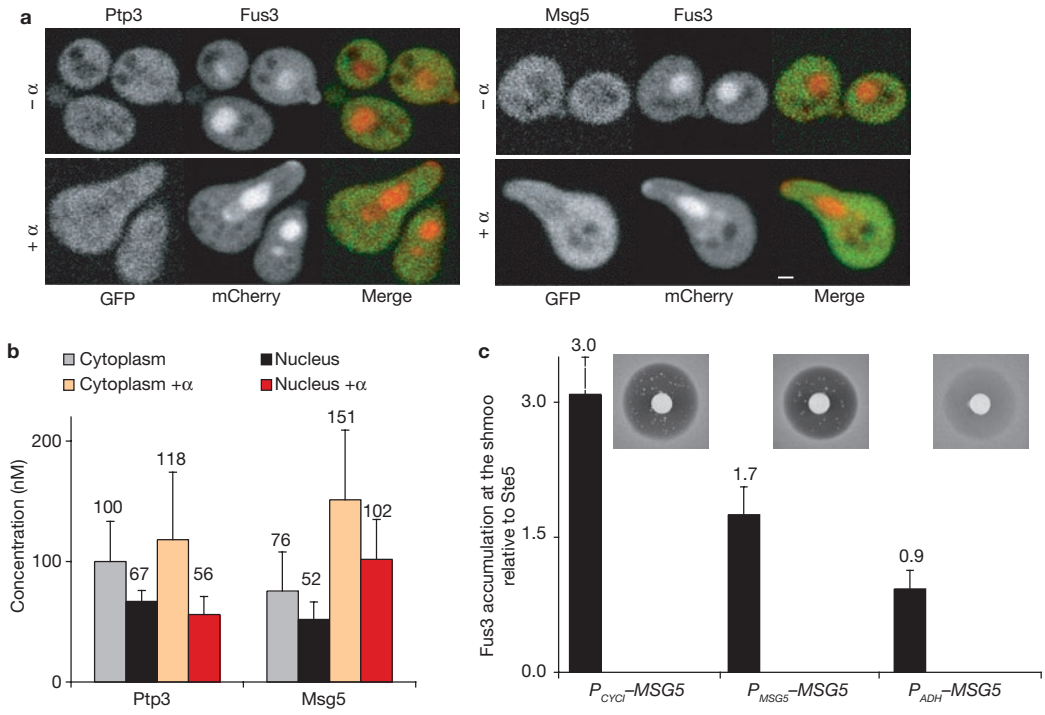

Figure 4 Cytoplasmic phosphatase levels influence the binding of Fus3 at the shmoo. (**a**) Distribution of the phosphatases Ptp3 and Msg5 and their target Fus3. Confocal microscopy images of 3meGFP-tagged Ptp3 and Msg5 coexpressed with Fus3–3mCherry in vegetative yeast cells and on stimulation with α-factor for 2.5–3 h. The scale bar represents 1 μm. (**b**) Concentrations of 3meGFP-tagged Ptp3 and Msg5 measured in the cytoplasm and nucleus of vegetative and α-factor stimulated cells (2.5–3 h). The values for the concentrations in the nucleus are likely to be slightly overestimated, due to partial overlap of the confocal volume with cytoplasmic areas (see Methods). The regions of the nucleus were identified using the Fus3–3mCherry localization (n = 16). Mean values and s.d. are shown. (**c**) Enrichment of Fus3 versus Ste5 is increased when Msg5 is underexpressed (P_{CYCI}–*MSG5*) and decreased on overexpression (P_{ADH}–*MSG5*) compared to cells with the endogenous expression level of Msg5 (P_{MSG5}–*MSG5*). Mean values and s.e.m. for 40–80 cells are shown. Halo assays (see Methods) are shown for the corresponding strains. Although the growth of P_{ADH}–*MSG5* cells was only partially inhibited, as revealed by the halo assay, microscopy revealed a substantial fraction of cells that arrested completely and formed proper shmoos after 2.5–3 h pheromone stimulation.

timescale of Fus3^{PP} across the cell. We investigated the possibility of a Fus3^{PP}-activity gradient using a reaction-diffusion model. The modelling parameters were based primarily on measured values from this work and from previously published studies (see Methods and Discussion) with only two unknowns: the Fus3 phosphorylation rate by activating kinases at the shmoo tip k (s^{-1}), and the Fus3 dephosphorylation rate by cytoplasmic phosphatases, p (s^{-1}). The contrast of cytoplasmic Fus3^{PP} activity at the distal end and at the nuclear position versus the region of the shmoo tip is determined solely by the dephosphorylation rate p ($= k_{cat}/K_M \cdot$ [ppase]) (Fig 5a), which requires $p < 15\ s^{-1}$ to ensure that active Fus3^{PP} can reach the nucleus (>1 Fus3^{PP} protein in the nucleus, considering the constitutive nuclear import of Fus3 independent of its phosphorylation state[5], which leads to a three-fold higher concentration of Fus3 in the nucleus). The measured concentration of Msg5 and Ptp3 in the cytoplasm ([ppase] = 0.26 μM), together with the typically reported substrate specificity constant for dual specificity phosphatases ($k_{cat}/K_M \approx 3.5\ \mu M^{-1}\ s^{-1}$)[19,20], resulted in a value of $p \approx 1\ s^{-1}$. This yielded a gradient of active Fus3^{PP} that matched the dimensions of a yeast cell, but was still flat enough to allow a substantial nuclear pool of active Fus3^{PP} (Fig. 5b).

To directly observe the Fus3^{PP} activity gradient, fluorescence resonance energy transfer (FRET) between Fus3–GFP and Cy3-labelled antibodies specific to the activated MAP kinases (anti-pTEpY–Cy3) was imaged by fluorescence lifetime imaging microscopy (FLIM[21]) in fixed cells. The lifetime profile across the cells (from the shmoo to the rear of the cell), averaged over several cells, revealed a gradient of active Fus3^{PP} emanating from the shmoo tip (Fig. 5c). The fluorescence lifetime increased towards the centre of the cell, where the nucleus resides, to the basal lifetime value, as observed in unstimulated cells (Fig. 5d; for controls of the FLIM experiment, see Supplementary Information Fig. S6a–c). In stimulated cells, active Fus3^{PP} levels were in the range of 40% of all Fus3 present (Fig. 5e). This value corresponds reasonably well with the amounts of active Fus3^{PP} as predicted by the simulation (roughly 25% for $p \approx 1\ s^{-1}$). Taken together, these results indicate that the shmoo is the source of active Fus3^{PP} and that counteracting phosphatases in the cytoplasm generate a gradient of Fus3^{PP} activity across the cell.

DISCUSSION

A gradient of active Fus3^{PP} in pheromone-stimulated and polarized cells may have several physiological roles. Most importantly, a gradient is able to maintain a local pool of activity. This leads to localized regulation of Fus3 targets, some of which are involved in cell polarity regulation, secretion and actin cable-based transport[22–28]. Therefore, morphological processes associated with shmoo formation and mating may rely on the precise distribution of Fus3 activity inside the cells. In stimulated cells, the gradient still allows for significant levels of active Fus3^{PP} in the

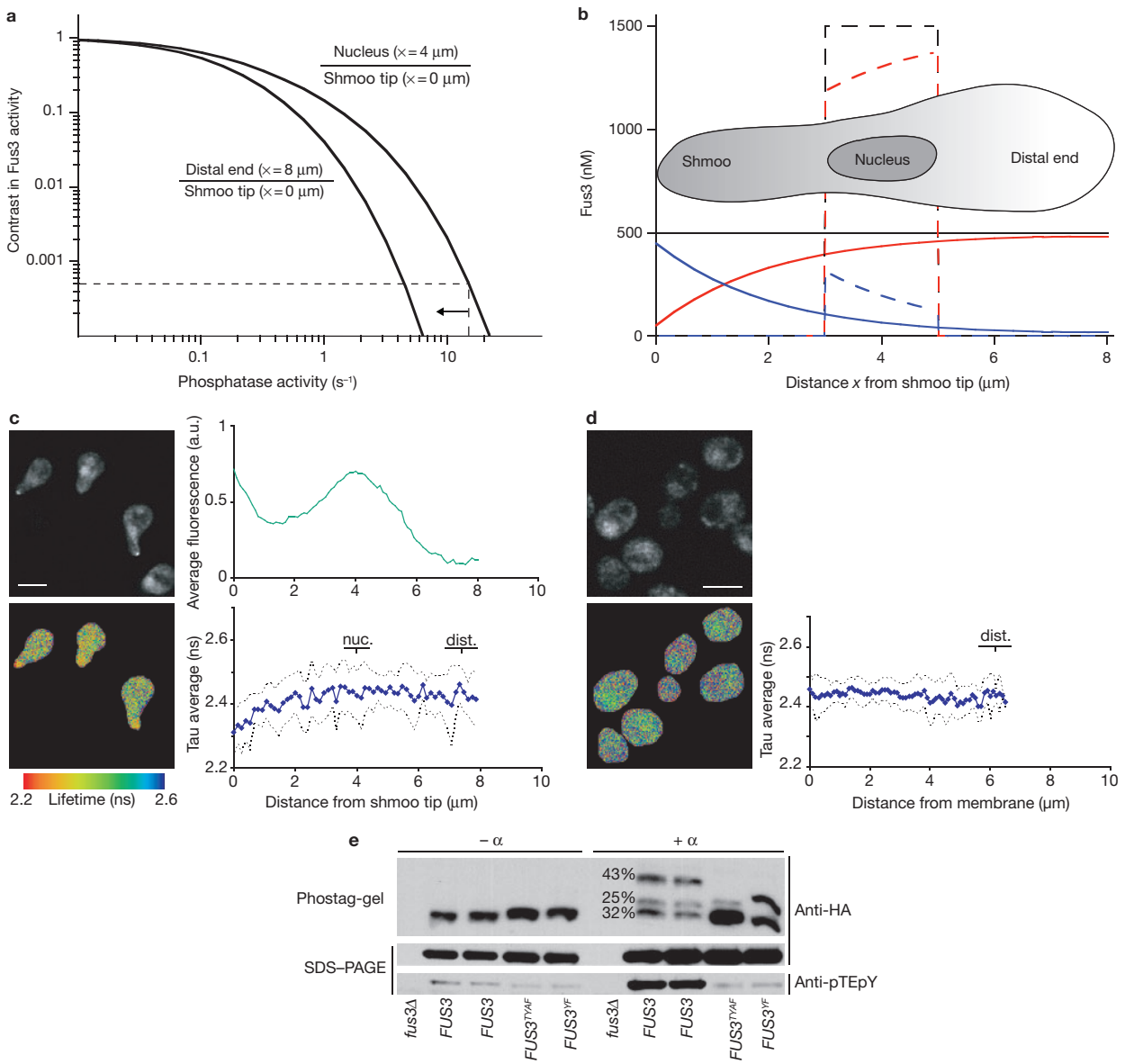

Figure 5 A gradient of active Fus3^{PP} emanates from the shmoo across the cytoplasm. (**a**, **b**) Computational analysis of a gradient of active Fus3^{PP}. The model tracks the cytoplasmic diffusion of Fus3, its binding and unbinding and phosphorylation at the shmoo tip, and its dephosphorylation by cytoplasmic phosphatases. The curves in **a** show the contrast of Fus3 activity (Fus3^{PP}) at the distal end of the cell and the nucleus versus the shmoo as a function of phosphatase activity. The arrow indicates the upper limit of phosphatase activity that still generates a physiologically relevant gradient (>1 molecule of Fus3^{PP} in the nucleus). The calculated gradient of active Fus3^{PP} for $p = 1$ s^{-1} in a stimulated, polarized yeast cell is shown in **b**. The distribution of the total (black), unphosphorylated (red) and phosphorylated (blue) Fus3 is indicated in the cytoplasm (solid lines) and in the nucleus (dashed lines), as a function of the distance from the shmoo tip (x). The model assumes phosphorylation of Fus3 at the shmoo tip (where Fus3 is rapidly turned over) and dephosphorylation in the cytoplasm (see Methods). (**c**, **d**) Visualization of the Fus3^{PP} gradient in stimulated cells. FLIM of phosphorylated Fus3^{PP} in non-stimulated and stimulated cells expressing Fus3–GFP. Fixed and permeabilized yeast cells were incubated with Cy3-labelled antibodies: (**c**) anti-pTEpY ($n = 63$ cells); (**d**) anti-pTEpY in non-stimulated cells ($n = 31$ cells). The GFP intensity images, the pseudocoloured fluorescence lifetime images and the plots displaying the fluorescence lifetime distribution averaged over several cells as a function of the distance from the shmoo tip are shown. The average position of the nucleus (nuc.) and the distal end of the cell (dist.) are indicated. The s.d. of the average lifetime values are plotted as dashed lines. For stimulated cells labelled with anti-pTEpY (**c**), the average normalized GFP intensity distribution is also indicated. The scale bars in **c** and **d** represent 5 μm. (**e**) The amounts of mono and diphosphorylated Fus3 (carboxy-terminallly tagged with 6HA) in vegetative and pheromone-stimulated cells (2.5–3 h) were quantified by phostag-gel electrophoresis (see Methods) followed by western blotting and immunodetection (using anti HA or anti-pTEpY antibodies, as indicated). Specificity of the anti-pTEpY antibody for the diphosphorylated form was demonstrated by SDS–PAGE with whole yeast cell extracts from unstimulated and stimulated cells.

region of the nucleus. The constitutive import of Fus3 into the nucleus, irrespective of its phosphorylation state[5], increases the concentration of active $Fus3^{PP}$ in the nucleus and ensures that significant levels of active $Fus3^{PP}$ are present there to regulate gene expression.

Nuclear positioning requires the action of the formin Bni1, which is activated by Fus3 and is responsible for the formation of actin cables that emanate from the shmoo[25]. These actin cables are necessary for proper microtubule orientation and nuclear positioning through their association with Kar9 and the myosin Myo2 (refs 29, 30). As Msg5 expression is induced by $Fus3^{PP}$ activity[15], the position of the nucleus and the gradient may constitute a regulatory system that enables regulation of nuclear positioning and transcriptional activity.

Our model of the spatiotemporal regulation of $Fus3^{PP}$ activity adds a new dimension to its role as a principal signal transducer in the pheromone response pathway. Future work will be required to understand the role of the $Fus3^{PP}$ activity gradient on the regulation of intracellular processes, and on the ability of cells to integrate external pheromone heterogeneities to precisely orient the shmoo and the site of cell–cell fusion. □

METHODS

Yeast strains, plasmids, cell extracts, gel electrophoresis and miscellaneous methods. Yeast strains used in this study are listed in Supplementary Information Table S1. Details on strain construction, plasmids and plasmid construction, yeast cell-extract preparation, antibodies and functionality assays are provided as Supplementary Information.

Fluorescence correlation/cross-correlation spectroscopy (FCS/FCCS). FCCS was performed using a TCS SP2-FCS system (Leica Microsystems, Wetzlar, Germany), as described in the Supplementary Information. The raw intensity data collected in the two detection channels (typically 3×10^5 photons) was auto- and cross-correlated, and analysed using the FCS Dataprocessor 1.5 software (SSTC, Minsk, Belarussia). Data for cells in which significant photobleaching, intracellular movement or high-blue autofluorescence was present were discarded. The curves were fit to a diffusion model that included additional terms for the photophysics of the fluorescent protein and an offset. The resulting concentrations were corrected for background fluorescence, crosstalk, dye maturation and the non-perfect overlap of the detection volumes, as described in Supplementary Information.

Confocal photon-counting (APD) imaging. Fluorescence confocal microscopy was performed on the Leica system described above using avalanche photodiode detectors (APDs). *z*-stacks of eight images per channel were taken consecutively at 400 nm step size. Each image was acquired by accumulating three frames. Laser powers were set to 4.8 μW (488 nm) and 5.6 μW (561 nm) for Ste5, Ste7 and Ste11, and 1.6 μW (488 nm) and 2.5 μW (561 nm) for Fus3. Images were processed with ImageJ (NIH, Bethesda, MA). For purpose of figure production, a Gaussian blur filter (width 1 pixel) was applied to each image followed by maximum projection and a linear brightness adjustment.

Quantitative image analysis. For quantitative analysis, confocal photon counting images were acquired at the equatorial plane of the yeast cells using the 488 nm (1.6 μW) and 561 nm laser lines (0.8 μW) in sequential mode. Each image was generated by averaging 20 single frames. With these settings, bleaching of the red and green fluorescent proteins was negligible. The images were corrected for background using images of cells that express no fluorescent proteins. The mean intensities of the shmoo tip, cytoplasm and nucleus were measured using ImageJ software. Regions of interest in the individual cells (shmoo, nucleus and cytoplasm) were outlined using the region tool of ImageJ. Because of the small thickness of the cell membrane in comparison to the optical resolution of the system, the intensity values at the shmoo tip were corrected for cytoplasmic contributions by subtracting the mean intensity of a cytoplasmic region that was equal in size to the measured shmoo tip region. The nuclear intensity was calculated from a small area in the centre of the nucleus in order to reduce cytoplasmic contamination. The mean fluorescence intensities were related to the corresponding concentrations of the fusion proteins in the cytoplasm, as determined by FCS (see Supplementary Information). The following strains were used to determine the shmoo accumulation of the different components: Ste5–3meGFP Fus3–3mCherry, Ste5–3mCherry Ste7–3meGFP and Ste5–3mCherry Ste11–3meGFP (strains YCM434, 439 and 446; see Supplementary Information, Table S1). To determine the amount of Ste7 and Ste11 in the nucleus, nuclear intensities were determined using either Fus3–3mCherry Ste11–3meGFP or Fus3–3mCherry Ste7–3meGFP cells (strains YCM436 and 435). The nuclear amounts of Ste11 and Ste7 were then related to the one of Ste5 determined in the Fus3–3mCherry Ste5–3meGFP strain (YCM434).

Fluorescence lifetime imaging (FLIM). FLIM measurements were performed in vegetative and pheromone-treated (3 h) Fus3–GFP expressing cells (strain YCM342). Cells were fixed with paraformaldehyde for 3 h and the cell walls were removed using zymolyase. For microscopy, cells were adsorbed on a poly-L-lysine-treated multiwell slide, permeabilized with 0.1% Triton X-100 and incubated with Cy3-labelled antibodies. FLIM measurements of GFP were performed in the presence of excess antibodies (see Supplementary Information). FLIM images were obtained using a Fluoview 1000 microscope (Olympus, Hamburg, Germany), equipped with a Picoharp 300 photon counting setup (Picoquant, Berlin, Germany). Images of 256 × 256 pixels were acquired over 4 min, corresponding to approximately 1 million detected photons. Images of the donor fluorescence were processed using the SymPhoTime software package (v4.2, Picoquant). The images were analysed on a pixel-by-pixel basis using a two-exponential fitting model including background. Both fluorescence lifetimes, corresponding to the populations of non- and interacting GFP proteins, were retrieved from analysis of the summed photon count histograms of control and sample (see Supplementary Information), and fixed during analysis. To visualize a gradient, the average fluorescence lifetime values were superimposed on an axis of symmetry in the yeast cell, starting at the shmoo tip and ending at the distal end of the cell.

The effective K_D (K_D^{eff}). To characterize the strength of interactions, an effective K_D (K_D^{eff}) can be defined. K_D^{eff} is based on the FCS/FCCS-measured concentrations and is defined under the assumption of a simple binary interaction. For each interaction, values of K_D^{eff} were calculated in single cells and were found to follow a log-normal distribution (see below). The assumption of simple binary interactions is inadequate to describe the macromolecular assembly of complexes among the various MAPK components. In such a scenario, K_D^{eff} is, in actuality, a function of multiple K_Ds and, more significantly, can depend on individual interactor concentrations (see Supplementary Information). However, it is still a useful measure of the amount of complex formation, allowing comparision across two cell populations with similar component concentration distributions, which is the case in our study of vegetative and short term-stimulated cells (<1 h). Here, protein abundances do not significantly change (Fig. 2) in contrast to long term stimulated cells, where Fus3 levels are increased ~threefold (see Supplementary Information, Fig. S2).

Log-normal distributions. The distributions of the single-cell FCS measurements of the effective interaction strengths followed log-normal distributions[31]. Taking the logarithm of these quantities removed the skewed tails to higher values found in regular units (see Supplementary Information, Fig. S3i), resulting in a symmetrical Gaussian profile in log units (see Supplementary Information, Fig. S3j). The mean, s.d. and s.e.m. of the logarithmic distribution was, therefore, much more reliable and meaningful than the same quantities obtained without taking the logarithm. These quantities were then converted back to the regular units by exponentiation: $\text{mean}_{log} = 10^{mean}$, $\text{s.d.}_{log} = 10^{s.d.}$, $\text{s.e.m.}_{log} = 10^{s.e.m.}$. The converted values s.d._{log} and s.e.m._{log} are scale factors. To obtain the upper (lower) 1σ values in regular units requires multiplication (division) by these quantities. To obtain the 2σ values requires multiplication or division by the square of these quantities, and so on. The statistics on all of the observed interactions are shown in the Supplementary Information, Table S2, including comparisons based on *P* values obtained using the Mann-Whitney U test (http://elegans.swmed.edu/~leon/stats/utest.html).

Fus3-activity gradient model. A simple one-dimensional model was used to model the Fus3 activity in the yeast cells. This included a spatial partitioning of Fus3 kinases (located at the shmoo tip) and Fus3 phosphatases (spread throughout

the cytoplasm). For such spatial partitioning, a gradient of Fus3 activity will form across the cell, with maximum activity at the shmoo tip and a contrast with other positions in the cytoplasm proportional to

$$\cosh\sqrt{p(L-x)^2/D}$$

where p is the phosphatase rate, $L = 8$ μm is the length of the cell (from shmoo tip to the distal end), x is the distance from the shmoo tip, and D is the diffusion constant of Fus3. Fig. 5a shows that the contrast in Fus3 activity (normalized to the shmoo tip) increases as a function of the phosphatase rate. In Fig. 5b, the gradient was plotted assuming $p = 1\ s^{-1}$ and a tenfold higher phosphorylation rate ($k = 10\ s^{-1}$) of Fus3 at the shmoo tip (further details are provided in the Supplementary Information).

Note: Supplementary Information is available on the Nature Cell Biology website.

ACKNOWLEDGEMENTS

We would like to thank R. Pepperkok, T. Zimmermann, J. Rietdorf, S. Terjung and A. Seitz of the advanced light microscopy facility (ALMF) of EMBL and L. Kuschel (Leica Microsystems, Germany) for their continuous support, and our reviewers for constructive comments. G. F. Fink is acknowledged for plasmid pBI479 (P_{FUS1}–lacZ) and W. A. Lim for plasmids containing *STE7* and *STE5* mutants.

Published online at http://www.nature.com/naturecellbiology/
Reprints and permissions information is available online at http://npg.nature.com/reprintsandpermissions/

1. Dohlman, H. G. & Thorner, J. W. Regulation of G protein-initiated signal transduction in yeast: paradigms and principles. *Annu. Rev. Biochem.* **70,** 703–754 (2001).
2. Inouye, C., Dhillon, N. & Thorner, J. Ste5 RING-H2 domain: role in Ste4-promoted oligomerization for yeast pheromone signaling. *Science* **278,** 103–106 (1997).
3. Garrenton, L. S., Young, S. L. & Thorner, J. Function of the MAPK scaffold protein, Ste5, requires a cryptic PH domain. *Genes Dev.* **20,** 1946–1958 (2006).
4. Winters, M. J., Lamson, R. E., Nakanishi, H., Neiman, A. M. & Pryciak, P. M. A membrane binding domain in the ste5 scaffold synergizes with gβγ binding to control localization and signaling in pheromone response. *Mol. Cell* **20,** 21–32 (2005).
5. van Drogen, F., Stucke, V. M., Jorritsma, G. & Peter, M. MAP kinase dynamics in response to pheromones in budding yeast. *Nature Cell Biol.* **3,** 1051–1059 (2001).
6. Cook, J. G., Bardwell, L., Kron, S. J. & Thorner, J. Two novel targets of the MAP kinase Kss1 are negative regulators of invasive growth in the yeast *Saccharomyces cerevisiae*. *Genes Dev.* **10,** 2831–2848 (1996).
7. Bacia, K., Kim, S. A. & Schwille, P. Fluorescence cross-correlation spectroscopy in living cells. *Nature Methods* **3,** 83–89 (2006).
8. Zhan, X. L., Deschenes, R. J. & Guan, K. L. Differential regulation of FUS3 MAP kinase by tyrosine-specific phosphatases PTP2/PTP3 and dual-specificity phosphatase MSG5 in *Saccharomyces cerevisiae*. *Genes Dev.* **11,** 1690–1702 (1997).
9. Wang, Y. & Elion, E. A. Nuclear export and plasma membrane recruitment of the Ste5 scaffold are coordinated with oligomerization and association with signal transduction components. *Mol. Biol. Cell* **14,** 2543–2558 (2003).
10. Madden, K. & Snyder, M. Cell polarity and morphogenesis in budding yeast. *Annu. Rev. Microbiol.* **52,** 687–744 (1998).
11. Sheu, Y. J., Santos, B., Fortin, N., Costigan, C. & Snyder, M. Spa2p interacts with cell polarity proteins and signaling components involved in yeast cell morphogenesis. *Mol. Cell Biol.* **18,** 4053–4069 (1998).
12. Remenyi, A., Good, M. C., Bhattacharyya, R. P. & Lim, W. A. The role of docking interactions in mediating signaling input, output, and discrimination in the yeast MAPK network. *Mol. Cell* **20,** 951–962 (2005).
13. Deminoff, S. J., Howard, S. C., Hester, A., Warner, S. & Herman, P. K. Using substrate-binding variants of the cAMP-dependent protein kinase to identify novel targets and a kinase domain important for substrate interactions in *Saccharomyces cerevisiae*. *Genetics* **173,** 1909–1917 (2006).
14. Bhattacharyya, R. P. *et al.* The Ste5 scaffold allosterically modulates signaling output of the yeast mating pathway. *Science* **311,** 822–826 (2006).
15. Doi, K. *et al.* MSG5, a novel protein phosphatase promotes adaptation to pheromone response in *S. cerevisiae*. *EMBO J.* **13,** 61–70 (1994).
16. Zhan, X. L. & Guan, K. L. A specific protein-protein interaction accounts for the *in vivo* substrate selectivity of Ptp3 towards the Fus3 MAP kinase. *Genes Dev.* **13,** 2811–2827 (1999).
17. Bastiaens, P., Caudron, M., Niethammer, P. & Karsenti, E. Gradients in the self-organization of the mitotic spindle. *Trends Cell Biol.* **16,** 125–134 (2006).
18. Kholodenko, B. N. Cell-signalling dynamics in time and space. *Nature Rev. Mol. Cell Biol.* **7,** 165–176 (2006).
19. Wang, Z. X., Zhou, B., Wang, Q. M. & Zhang, Z. Y. A kinetic approach for the study of protein phosphatase-catalyzed regulation of protein kinase activity. *Biochemistry* **41,** 7849–7857 (2002).
20. Zhao, Y. & Zhang, Z. Y. The mechanism of dephosphorylation of extracellular signal-regulated kinase 2 by mitogen-activated protein kinase phosphatase 3. *J. Biol. Chem.* **276,** 32382–32391 (2001).
21. Bastiaens, P. I. & Squire, A. Fluorescence lifetime imaging microscopy: spatial resolution of biochemical processes in the cell. *Trends Cell Biol.* **9,** 48–52 (1999).
22. Elion, E. A., Satterberg, B. & Kranz, J. E. FUS3 phosphorylates multiple components of the mating signal transduction cascade: evidence for STE12 and FAR1. *Mol. Biol. Cell* **4,** 495–510 (1993).
23. Lew, D. J. Yeast polarity: negative feedback shifts the focus. *Curr. Biol.* **15,** R994–R996 (2005).
24. Li, E., Cismowski, M. J. & Stone, D. E. Phosphorylation of the pheromone-responsive Gβ protein of *Saccharomyces cerevisiae* does not affect its mating-specific signaling function. *Mol. Gen. Genet.* **258,** 608–618 (1998).
25. Matheos, D., Metodiev, M., Muller, E., Stone, D. & Rose, M. D. Pheromone-induced polarization is dependent on the Fus3p MAPK acting through the formin Bni1p. *J. Cell Biol.* **165,** 99–109 (2004).
26. Metodiev, M. V., Matheos, D., Rose, M. D. & Stone, D. E. Regulation of MAPK function by direct interaction with the mating-specific Gα in yeast. *Science* **296,** 1483–1486 (2002).
27. Ozbudak, E. M., Becskei, A. & van Oudenaarden, A. A system of counteracting feedback loops regulates Cdc42p activity during spontaneous cell polarization. *Dev. Cell* **9,** 565–571 (2005).
28. Qi, M. & Elion, E. A. Formin-induced actin cables are required for polarized recruitment of the Ste5 scaffold and high level activation of MAPK Fus3. *J. Cell Sci.* **118,** 2837–2848 (2005).
29. Hwang, E., Kusch, J., Barral, Y. & Huffaker, T. C. Spindle orientation in *Saccharomyces cerevisiae* depends on the transport of microtubule ends along polarized actin cables. *J. Cell Biol.* **161,** 483–488 (2003).
30. Yin, H., Pruyne, D., Huffaker, T. C. & Bretscher, A. Myosin V orientates the mitotic spindle in yeast. *Nature* **406,** 1013–1015 (2000).
31. Limpert, E., Stahel, W. A. & Abbt, M. Log-normal distributions across the sciences: Keys and clues. *Bioscience* **51,** 341–352 (2001).

nature cell biology

SUPPLEMENTARY INFORMATION

Spatial regulation of Fus3 MAP kinase activity through a reaction-diffusion mechanism in yeast pheromone signaling

Celine I Maeder[1*], Mark A Hink[2*], Ali Kinkhabwala[2], Reinhard Mayr[1,3], Philippe I H Bastiaens[2] & Michael Knop[1]
* These authors contributed equally to this work.

[1] EMBL, Meyerhofstrasse 1, 69117 Heidelberg, Germany
[2] Max-Planck-Institute for Molecular Physiology, Dept. of Systemic Cell Biology, Otto-Hahn-Str. 11, 44227 Dortmund, Germany
[3] present address: Upper Austrian Research GmbH
Center for Biomedical Nanotechnology (CBN)
Scharitzerstraße 6-8, 4020 Linz, Austria
Correspondence should be addressed to MK (knop@embl.de) or PIHB (philippe.bastiaens@mpi-dortmund.mpg.de)

1.1. Yeast methods and reagents

1.1.1. Yeast strains, PCR targeting of yeast genes, growth media and growth conditions

The genotypes of the strains used in this work are listed in Supplementary Table S1. Basic yeast methods and growth media are described elsewhere[1]. For alpha factor treatment, cells were pre-grown in liquid YPD or synthetic complete (SC) medium and alpha factor was added to final 10 $\mu g \cdot ml^{-1}$. For cycloheximide chase experiments, cycloheximide (Sigma) was directly dissolved in SC medium to final concentration of 1 $mg \cdot ml^{-1}$.

All yeast strains used in this study are derivatives of the S288c strain ESM356-1 (see Supplementary Table S1). Chromosomal manipulations of yeast strains (C-terminal tagging, gene deletions and promoter substitutions) were performed using PCR amplified cassettes as described previously[2]. Cassettes used for PCR targeting were constructed as described[2] using cDNA of meGFP, tdTomato and mCherry (details, plasmids and sequences available upon request; see also next point 1.1.2.). Correct integration of the cassettes into the genome of yeast strains was tested by PCR and fluorescence microscopy, the expression of full-length tagged proteins with the expected molecular weight was validated using Western blotting.

For the construction of strains expressing wild type *FUS3* together with mutant *FUS3* alleles (*FUS3DDKK, FUS3TYAF* and *FUSK42R*), the integrative plasmid pRS306K[3] containing the specific alleles, tagged with three copies of meGFP (see Section 1.1.2), was linearized and integrated into the *URA3* locus (yeast strains YCM549, 562, 563 and 564). Further details on plasmids are available upon request. The mutant alleles were obtained by Quickchange mutagenesis of the wild type *FUS3* gene.

For replacement of wild type genes with mutant alleles on the chromosome, the gene, or a region of it, was first deleted using a *natNT2-klURA3* double selection marker in the strain with the desired genetic background. Such deletion strains were then transformed with DNA fragments containing either the wild type or mutant allele of the gene. For *STE5ND* and *STE7ND1ND2,* DNA fragments cut out from published plasmids were used[4, 5]. For *FUS3* mutant alleles, DNA fragments containing the entire *FUS3* open reading frame were derived from the pRS306K variants described in the previous paragraph. For *STE5VASP* and *STE5FL* mutant alleles, the corresponding region of *STE5* was cloned into a plasmid and mutagenized by Quickchange PCR.

Clones were selected on 5'-FOA and confirmed first by the absence of the *natNT2* marker and second by PCR and sequencing.

For microscopy, yeast cells grown in log phase (approx. $0.5 \cdot 10^7$ $cells \cdot ml^{-1}$) were immobilized in glass bottomed well chambers (Lab-Tek 155411; Nalce Nunc Int., USA). The chambers were pre-treated for at least 30 minutes with Bioconect (UCT, USA) followed by one ethanol and one water wash step and incubation for >30 minutes with 6% ConcanavalinA (C2010; Sigma, Germany), followed again by two wash steps with water.

1.1.2. Fluorescent protein constructs

C-terminally tagged proteins contain three copies of either GFP or mCherry. Spacer sequences between the tagged protein and the first copy of GFP were RTLQVDGS, and RTLQVD in the case of mCherry[6]. The GFP domains were spaced using GS and the mCherry domains using LD. The particular GFP variant used (named meGFP, for monomeric enhanced GFP) was a yeast codon optimized version of GFP [7] containing the following mutations (as compared to the original GFP)[7, 8]:

S65G, S72A, R80Q, A206R. For FLIM, Fus3 was C-terminally tagged using PCR tagging with EGFP (Clonetech) on plasmid pYM28[2].

1.1.3. Antibodies

Antibodies specific for meGFP was produced in rabbits and affinity purified. Anti-pTEpY (anti-phospho ERK1/2) was purchased from R&D systems (AF1018). Goat anti-mouse/rabbit Alexa-680 from Molecular Probes was used as secondary antibody for quantitative Western blotting. Donkey-anti-rabbit Cy3 was purchased from Jackson ImmunoResearch Laboratories Inc.

1.1.4. Cell lysis and gel electrophoresis

Yeast cell extracts using denaturing conditions were prepared as described elsewhere[9]. Phos-tag SDS-PAGE was performed as described using a 10% gel[10]. Proteins were transferred to PDVF membranes using tank blotting. For quantitative Western blot analysis secondary antibodies labeled with Alexa680 were used for visualization. Detection was performed with the Odyssey Infrared Imaging System (LI-Cor Biosystems, Germany). Membranes were scanned at 700 nm at 169 μm resolution, medium quality; focus offset of 3.0 mm was used and the intensity setting was set to four. Images were quantified using ImageJ software.

1.1.5. Functionality assays

Halo assays and transcriptional response assays were performed as described elsewhere[11]. Double-labeled MAPK strains were transformed with pBI497 (pFUS1-βGAL) and β-galactosidase activity was measured before and after 90 minutes of α-factor stimulation (final concentration of 10 $\mu g \cdot ml^{-1}$). Results are shown in Supplementary Fig. S1.

1.1.6. Table S1 with yeast strains

Strain	Genotype	Source
ESM356-1	*MAT*a *ura3-53 leu2Δ1 his3Δ200 trp1Δ63* (parental strain for all strain constructions)	Ref.[12]
YCM58	*sst1Δ::hphNT1*	this study
YCM84	*STE5::3meGFP::kanMX*	this study
YCM85	*STE7::3meGFP::kanMX*	this study
YCM86	*STE11::3meGFP::kanMX*	this study
YCM95	*natNT2::P_{ADH}::eGFP::DON1*	this study
YCM315	*STE11::tdTomato::hphNT1*	this study
YCM342	*FUS3::EGFP::HIS3 sst1Δ::hphNT1*	this study
YCM392	*FUS3::3mCherry::hphNT1*	this study
YCM403	*STE5::3meGFP::kanMX STE11::3mCherry::hphNT1*	this study
YCM404	*STE7::3meGFP::kanMX STE11::3mCherry::hphNT1*	this study
YCM405	*STE5::3myeGFP::kanMX FUS3::3mCherry::hphNT1*	this study
YCM406	*STE7::3meGFP::kanMX FUS3::3mCherry::hphNT1*	this study
YCM407	*STE11::3meGFP::kanMX FUS3::3mCherry::hphNT1*	this study
YCM411	*STE7::3meGFP::kanMX STE5::3mCherry::hphNT1*	this study
YCM413	*STE11::3meGFP::kanMX STE5::3mCherry::hphNT1*	this study
YCM419	*STE11::3mCherry::hphNT1*	this study
YCM432	*STE5::3meGFP::kanMX STE11::3mCherry::hphNT1*	this study

	sst1Δ::natNT2	
YCM434	*STE5::3meGFP::kanMX FUS3::3mCherry::hphNT1 sst1Δ::natNT2*	this study
YCM435	*STE7::3meGFP::kanMX FUS3::3mCherry::hphNT1 sst1Δ::natNT2*	this study
YCM436	*STE11::3meGFP::kanMX FUS3::3mCherry::hphNT1 sst1Δ::natNT2*	this study
YCM439	*STE7::3meGFP::kanMX STE5::3mCherry::hphNT1 sst1Δ::natNT2*	this study
YCM458	*STE7::3meGFP::kanMX STE11::3mCherry::hphNT1 sst1Δ::natNT2*	this study
YCM446	*STE11::3meGFP::kanMX STE5::3mCherry::hphNT1 sst1Δ::natNT2*	this study
YCM449	*natNT2::PcycI::eGFP::DON1::3mCherry::kanMX*	this study
YCM452	*natNT2::PcycI::eGFP::DON1 STE11::3mCherry::hphNT1*	this study
YCM465	*pRS406- P_{CYCI}::meGFP::T_{CYCI}*	this study
YCM472	*natNT2::P_{CYCI}::DON1::meGFP::kanMX*	this study
YCM474	*natNT2::P_{CYCI}::DON1::3meGFP::kanMX*	this study
YCM498	*MSG5::3meGFP::natNT2 FUS3::3mCherry::hphNT1, sst1Δ::kanMX*	this study
YCM498	*PTP3::3meGFP::natNT2 FUS3::3mCherry::hphNT1, sst1Δ::kanMX*	this study
YCM549	*sst1Δ::HIS3MX6 FUS3::3mCherry::hphNT1 ura3::P_{FUS3}::FUS3::3meGFP::T_{CYCI}::kanMX::ura3*	this study
YCM562	*sst1Δ::HIS3MX6 FUS3::3mCherry::hphNT1 ura3::P_{FUS3}::FUS3^{K42R}::3meGFP::T_{CYCI}::kanMX::ura3*	this study
YCM563	*sst1Δ::HIS3MX6 FUS3::3mCherry::hphNT1 ura3::P_{FUS3}::FUS3^{D314K,D317K}::3meGFP::T_{CYCI}::kanMX::ura3*	this study
YCM564	*sst1Δ::HIS3MX6 FUS3::3mCherry::hphNT1 ura3::P_{FUS3}::FUS3^{T180A,Y182F}::3meGFP::T_{CYCI}::kanMX::ura3*	this study
YCM581	*FUS3::6HA::kanMX sst1Δ::HIS3MX6*	this study
YCM582	*sst1Δ::HIS3MX6 FUS3::3mCherry::hphNT1 STE5::3meGFP::kanMX*	this study
YCM583	*sst1Δ::HIS3MX6 FUS3^{D314K,D317K}::3mCherry::hphNT1 STE5::3meGFP::kanMX*	this study
YCM584	*sst1Δ::HIS3MX6 FUS3::3mCherry::hphNT1 STE7::3meGFP::kanMX*	this study
YCM585	*sst1Δ::HIS3MX6 FUS3^{K42R}::3mCherry::hphNT1 STE7::3meGFP::kanMX*	this study
YCM586	*sst1Δ::HIS3MX6 FUS3^{D314K,D317K}::3mCherry::hphNT1 STE7::3meGFP::kanMX*	this study
YCM587	*sst1Δ::HIS3MX6 FUS3^{T180A,Y182F}::3mCherry::hphNT1 STE7::3meGFP::kanMX*	this study
YCM591	*fus3Δ::klURA::natNT2 sst1Δ::HIS3MX6*	this study
YCM598	*sst1Δ::HIS3MX6 FUS3^{K42R}::3mCherry::hphNT1 STE5::3meGFP::kanMX*	this study

YCM599	*sst1Δ::HIS3MX6 FUS3^{T180A,Y182F}::3mCherry::hphNT1 STE5::3meGFP::kanMX*	this study
YCM601	*sst1Δ::HIS3MX6 FUS3::3mCherry::hphNT1 STE5::3meGFP::kanMX*	this study
YCM602	*sst1Δ::HIS3MX6 FUS3::3mCherry::hphNT1 STE5$^{Q292A, I294A, Y295A, L307A, P310A, N315A}$::3meGFP::kanMX*	this study
YCM609	*FUS3 ^{T180A,Y182F}::6HA::kanMX, sst1Δ::HIS3MX6*	this study
YCM610	*FUS3^{Y182F}::6HA::kanMX, sst1Δ::HIS3MX6*	this study

1.2. Microscopic methods and measurements and additional discussions of results

1.2.1. General remarks on fluorescence (cross-) correlation spectroscopy (FCS/FCCS) in yeast cells

The most critical experimental parameter that determines the quality of fluorescence correlation curves is the molecular brightness of the labeled proteins. We have therefore used triple fusions of fluorescent proteins (yeast enhanced monomeric GFP (3meGFP) or mCherry (3mCherry)[6] (Fig S3d). meGFP and mCherry is a good pair for dual-color cross-correlation measurements since the proteins are sufficiently fast maturing, not very sensitive to photobleaching and their emission spectra are well separated. Using a cycloheximide chase, we determined that only 50% of the mCherry tagged proteins are fluorescent (see Supplementary Information Fig. S3c), and all our results were corrected accordingly. To establish FCCS, we first used cells expressing a positive control consisting of a fusion of eGFP and 3mCherry separated by a neutral spacer protein, Don1 (Don1 is a meiotic protein that distributes uniformly upon ectopic expression in vegetative cells. By using 2-hybrid, we found no self-interaction of Don1, and by using photon counting histogram analysis (PCH), we confirmed that molecular brightness of Don1-GFP is equal do GFP, when expressed in cells (Supplementary Fig. S3d). This confirms the monomeric nature of Don1.). Typical auto- and cross-correlation curves are shown in Supplementary Information Fig. S3e, f. We obtained an average cross-correlation amplitude over many cells corresponding to 77% complex (see Supplementary Information Fig. S3e). Using Western blotting, we found no indication of proteolytic cleavage of the eGFP-Don1-3mCherry protein, which would lead to the separation of the fluorophores (data not shown). Therefore the failure to detect 100% cross-correlation arose from imperfect overlap of the two confocal detection volumes at the respective excitation wavelengths. We corrected all our data for the non-perfect overlap. By contrast, no significant cross-correlation was observed for the negative control, where eGFP and 3mCherry were fused to different proteins that do not interact with each other (see Supplementary Information Fig. S3f). We verified that the type of fluorescent tag fused to an individual protein did not influence the determined protein or complex concentrations (see Supplementary Information Fig. S3g, h). We conclude that FCCS is a valid method to measure protein complex formation at low expression levels in living yeast cells. Further technical details on the used instruments and filters and on data analysis are provided in the next two sections.

1.2.2. FCS/FCCS data acquisition

Fluorescence correlation and fluorescence cross-correlation spectroscopy was performed using unbudded cells (in vegetative and pheromone stimulated populations) that are in G1 of the cell cycle and are therefore able to respond to pheromone stimulation[13]. The experiments were performed using a TCS SP2-FCS system (Leica Microsystems, Germany). meGFP was excited with the 488 nm line of an argon laser and mCherry was excited using a 561 nm diode laser. The laser power was set not higher than 2.5 kW·cm^{-2} (488 nm) and 3.5 kW·cm^{-2} (561 nm) respectively in order to minimize photobleaching, cellular damage and photophysical effects of the fluorescent proteins. The excitation light was focused by a water immersion Apochromat 63x objective lens (N.A. 1.2) into the sample. The emission light passed an adjustable pinhole that was set to 1 Airy unit. A filtercube containing a dichroic filter, LP560, was used to separate the emitted light into two different detection channels where BP500-550 and HQ638DF75 bandpass filters (Omega, USA) were used for spectral selection (see Supplementary Information Fig. S3a). The fluorescence was detected by avalanche photodiodes (APDs) (Perkin-Elmer Optoelectronics, Canada) that were coupled to a photon counting card (ISS, USA) allowing storage of the raw intensity data (typically 3·10^5 photons) in photon delay mode[14]. After each measurement of a single cell the filtercube was exchanged for a filtercube containing a BP460DF60 emission filter (AHF, Germany) in order to measure autofluorescence of the cell upon 405 nm diode excitation at the same location (blue autofluorescence, see next section).

1.2.3. FCS/FCCS data analysis

The raw data files were correlated and analyzed using the FCS Dataprocessor 1.5 software (SSTC, Belarussia,[15]). Files were discarded when significant photobleaching was apparent. To account for occasional cells with a high non-specific background, we measured for each cell the blue autofluorescence, which we found to correlate with autofluorescence levels in the green and red channel, when looking at cells without any fluorescent protein expressed (see Supplementary Information Fig. S3b). When the autofluorescence in the green or red channel (as determined using wild type cells) contributed more than 20% to the total intensity of in one or both of the measured channels, the blue autofluorescence value of this cell was checked. Cells with blue autofluorescence intensity that exceeded the average value plus the standard deviation as obtained in wild type cells were discarded from the analysis. Auto- and cross-correlation curves, G_{ij}, were generated from sections of the raw intensity trace, I, that were not obscured by intensity drifts due to photobleaching or intracellular movement:

$$G_{ij}(\tau) = 1 + \frac{< \delta I_i(t) \cdot \delta I_j(t+\tau) >}{< I_i > \cdot < I_j >} \quad \text{(with i=j for autocorrelation).} \qquad (1)$$

The autocorrelation curves of the green and red channels, G_{gg} and G_{rr}, were fitted between 100 μs and 100 ms according to a diffusion model including terms for the photophysics of the fluorescent protein[16] and an offset, G_∞, to compensate for small intensity drifts. T represents the fraction of molecules in the dark state and τ_T the relaxation rate of this dark state. The diffusion time of the fluorescent particles, τ_{dif}, depends on the shape of the observation volume, sp, that is defined as the ratio of the axial (ω_z) over the radial axis (ω_{xy}).

$$G_{ij}(\tau) = 1 + \left(1 - \frac{I_{i,\,background}}{I_{i,\,total}}\right)\left(1 - \frac{I_{j,\,background}}{I_{j,\,total}}\right) \cdot \left(\frac{1}{<N>} \cdot \frac{1 - T + Te^{\left(-\tau/\tau_T\right)}}{(1-T)} \cdot \frac{1}{\left(1 + \frac{\tau}{\tau_{dif}}\right)\sqrt{1 + \frac{\tau}{sp^2 \cdot \tau_{dif}}}} \right) + G_\infty \qquad (2)$$

The particle number, N, retrieved from this analysis has been corrected for background fluorescence using the first two terms between brackets in equation 2. These terms were used to correct the cross-correlation curves as well. Since it was not possible to measure or estimate the green and red autofluorescence level in each individual cell due to the presence of the fluorescent fusion proteins, the average autofluorescence obtained in wild type yeast was taken. Since there was no significant change in brightness upon binding, the amplitude of the cross-correlation curve, $G_{rg}(0)$, scales linearly to the concentration of the complex, C_{rg} (Schwille and Haustein; www.biophysics.org/education/schwille.pdf):

$$C_{rg} = \frac{G_{rg}(0)}{G_{gg}(0) \cdot G_{rr}(0) \cdot V_{rg}}, \qquad (3)$$

where V_{rg} is the effective cross-correlation observation volume. The obtained numbers for the red channel and the complex were corrected for the 50% maturation of mCherry (see Supplementary Information, Fig. S3c). Moderate photobleaching, only present in a minority of the mCherry traces, was corrected[17]. Further corrections included the 8% (non-correlating) crosstalk of the eGFP into the mCherry channel (present as an additional background signal) and the non-perfect overlap of the detection volumes, as determined from the positive control (see Supplementary Information, Fig. S3e). The resulting particle numbers were converted into concentration values by division through the size of the green, red or cross-correlation observation volume. The latter values were determined from calibration measurements with Alexa488 (green), Alexa546 (red) and Rhodamine Green (cross) (Invitrogen-Molecular Probes, USA) for which the diffusion coefficients, D, were known (260, 230 and 260 $\mu m^2.s^{-1}$ respectively):

$$\tau_{dif} = \frac{\omega_{xy}^2}{4D}. \qquad (4)$$

The observation volume was approximated by a cylinder using the structural parameter sp that was retrieved from the calibration analysis.

$$V = 2\pi\omega_{xy}^3 \cdot sp. \qquad (5)$$

The molecular brightness of the fusion proteins in yeast was studied using photon counting histogram (PCH)[18] and photon cumulant analysis (PCA)[19]. The data was binned to 5 kHz and analyzed using two-component models where the number of molecules and brightness of the first component was fixed to the average value obtained in autofluorescent wild type cells.

1.2.4. Additional controls and discussion of FCCS measurements

The magnitudes of the K_D^{eff} values obtained from measurements in vegetative and pheromone stimulated cells (Figure 2) indicate that the Ste5-Ste11 interaction is the strongest (0.05 μM), followed by the Ste5-Ste7 (0.1 μM) and Ste7-Fus3 (0.2 μM) interactions. The other three interactions, Ste7-Ste11, Ste11-Fus3 and Ste5-Fus3, are significantly weaker (~ 0.6 – 1.0 μM).

For controls, we have measured also the interaction of Ste7 with Ste7-binding-impaired Ste5 (Ste5VASP) and of Ste11 with Ste11-binding-impaired Ste5 (Ste5F514L). In addition, the interaction of Fus3 with a Fus3-binding-impaired mutant of Ste7 (Ste7ND1/2) was investigated.

In all cases a significantly decreased affinity of the interaction partners was observed (Figure S4), as expected from the publications that report these mutations[5, 20]. Detailed information about the measurements is provided in the Supplementary Table S2. We noticed still significant interaction between Ste5F514L and Ste11, in contrast to what was reported by means of biochemistry. However, these previous experiments were performed using strong overexpression conditions[20], whereas our measurements were done using endogenous protein level expression. We hypothesize that the Ste5-Ste11 interaction is helped by additional proteins (e.g. Ste20, Ste50 and maybe even Ste7), leading to the formation of significant amounts of common complexes even in the absence of a direct Ste5-Ste11 interaction. Under overexpression conditions, these factors simply become limiting. Our definition of interaction strength (the "effective K_D", K_D^{eff}) considers such situations, and Section 1.3.1. in Supplementary Information provides a theoretical framework for this phenomenon (cooperative binding).

1.2.5. Table S2: Statistical analysis of the FCS/FCCS measurements

Supplementary Table S2 Statistical analysis of FCS and FCCS data sets (corresponding to the results shown in Figures 2, 3c and Supplementary Fig. S4)

Exp. #	Green: 3meGFP Red: 3mCherry	α[1]	N[2]	Green nM	SD nM	SE nM	GC[3]	SD_{log}[5]	SE_{log}[5]	Red nM	SD nM	SE nM	RC[4]	SD_{log}[5]	SE_{log}[5]	Complex nM	SD nM	SE nM	K_D^{eff} nM	SD_{log}[5]	SE_{log}[5]	*P* (2-sided)[6], involving values from the two indicated exps.	
1	Ste11-Ste 5	-	16	40	21	5	0.19	1.61	1.13	27	20	5	0.33	1.42	1.09	8.3	5.5	1.4	54	1.84	1.16		
2	Ste11-Ste 5	+	40	33	13	2	0.17	1.56	1.07	23	17	3	0.29	1.63	1.08	6.3	4.4	0.7	54	2.60	1.16	**0.89**	1 & 2
3	Ste11-Ste5F514L	-	39	38	10	2	0.13	1.44	1.06	41	13	2	0.12	1.46	1.06	5.2	2.5	0.4	231	1.68	1.09	**<0.000002**	1 & 3
4	Ste11-Ste5F514L	+	28	31	10	2	0.11	1.35	1.06	31	8	2	0.11	1.49	1.07	3.4	1.7	0.3	224	1.54	1.09	**<0.000002**	2 & 4
5	Ste5-Ste1 1	-	14	38	18	5	0.19	1.66	1.15	47	38	10	0.17	2.27	1.24	8.4	6.1	1.6	128	3.24	1.37		
6	Ste5-Ste1 1	+	92	30	16	2	0.14	2.39	1.10	40	43	4	0.14	2.67	1.11	5.4	4.7	0.5	120	3.43	1.14	**0.55**	5 & 6
7	Ste7-Ste5	-	28	63	22	4	0.09	1.72	1.11	23	10	2	0.27	1.86	1.12	6.8	4.9	0.9	129	2.26	1.17		
8	Ste7-Ste5	+	23	54	17	3	0.07	1.91	1.15	15	8	2	0.28	1.98	1.15	4.2	2.0	0.4	107	3.06	1.26	**0.56**	7 & 8
9	Ste7-Ste5VASP	-	47	76	22	3	0.03	2.25	1.13	45	12	2	0.05	2.27	1.12	2.7	3.0	0.4	1421	3.09	1.18	**<0.000002**	7 & 9
10	Ste7-Ste5VASP	+	24	95	24	5	0.03	2.00	1.15	48	9	2	0.05	1.96	1.14	3.0	2.0	0.4	1505	2.12	1.17	**<0.000002**	8 &10
11	Ste7-Ste1 1	-	19	69	37	8	0.04	3.07	1.29	34	13	3	0.07	2.99	1.29	3.5	3.2	0.7	721	3.14	1.30		
12	Ste7-Ste1 1	+	51	83	40	6	0.04	1.80	1.09	38	23	3	0.09	2.25	1.12	4.2	3.5	0.5	657	2.34	1.13	**0.88**	11 &12
13	Ste5-Fus 3	-	24	52	11	2	0.15	1.93	1.14	170	57	12	0.05	1.94	1.15	9.6	8.4	1.7	837	2.27	1.18		
14	Ste5-Fus 3	+	16	52	21	5	0.11	1.92	1.18	146	49	12	0.04	2.22	1.22	7.1	5.4	1.4	980	2.39	1.24	**0.58**	13 & 14
15	Ste5ND-Fus 3	-	12	50	24	10	*n.d.*	*n.d.*	*n.d.*	155	55	22	*n.d.*	*n.d.*	*n.d.*	3.1	2.1	0.9	>2400	1.86	1.29	**<0.00013**	13 & 15
16	Ste11-Fus3	-	81	34	15	2	0.19	2.24	1.09	180	90	10	0.04	2.06	1.08	6.5	6.6	0.7	594	2.71	1.12		
17	Ste11-Fus3	+	63	28	18	2	0.17	2.62	1.13	197	186	24	0.03	3.29	1.16	5.9	5.9	0.7	597	3.81	1.18	**0.68**	16 & 17
18	Ste7-Fus 3	-	62	71	29	4	0.41	1.63	1.06	186	67	8	0.15	1.54	1.06	29.3	13.3	1.7	174	2.90	1.14		
19	Ste7-Fus 3	+	14	56	26	7	0.49	1.35	1.08	217	66	18	0.12	1.65	1.14	29.0	17.6	4.7	174	1.87	1.18	**0.63**	18 & 19
20	Ste7ND1.2-Fus3	-	25	42	14	3	0.06	2.23	1.17	183	39	8	0.01	2.09	1.16	3.1	2.9	0.6	2796	2.36	1.19	**<0.000002**	18 & 20
21	Ste7ND1.2-Fus3	+	39	44	14	2	0.04	1.97	1.11	163	46	7	0.01	2.01	1.11	2.1	1.6	0.2	3606	2.12	1.13	**<0.000002**	19 & 21
22	Ste7-Fus3K42R	-	23	59	15	3	*n.d.*	*n.d.*	*n.d.*	394	83	17	*n.d.*	*n.d.*	*n.d.*	39.7	15.4	3.2	128	2.83	1.24	**0.16**	18 & 22
23	Ste7-Fus3TYAF	-	22	72	18	4	*n.d.*	*n.d.*	*n.d.*	444	63	13	*n.d.*	*n.d.*	*n.d.*	51.1	14.7	3.1	154	1.80	1.13	**0.27**	18 & 23
24	Ste7-Fus3DDKK	-	25	66	21	4	*n.d.*	*n.d.*	*n.d.*	464	101	20	*n.d.*	*n.d.*	*n.d.*	29.1	11.8	2.4	429	3.12	1.26	**0.00006**	18 & 24

Grey shaded area: Values used for Figure 2 and Supplementary Figure S4 construction
Light blue shaded area: Values used for Figure 3c construction

1) addition of α-factor
2) N denotes the number of single cell measurements. Each single-cell measurement is considered to be one experiment. In case the experiments were conducted during the course of more than one day, the performance and the proper calibration of the instruments was checked on each day using positive and negative controls for the FCCS measurements (Supplementary Figure S3e and f).
3) Green in Complex (GC): fraction of the protein indicated in green (= 3meGFP tagged), that is in complex with the protein indicated in red (=3mCherry tagged)
4) Red in Complex (RC): fraction of the protein indicated in red (= 3mCherry tagged), that is in complex with the protein indicated in green (=3meGFP tagged)
5) SD and SE denote Standard Deviation and Standard Error, log denotes that the corresponding values are scaling factors (see Materials and Methods)
6) statistical analysis to investigate whether the difference of the interaction strength of two proteins (K_D^{eff}) in different strain backgrounds, or between mutant and wild type proteins, is significantly different.

n.d. not calculated

1.2.6. Self-interaction of Ste5 in the cytoplasm

Self-interaction of Ste5 has been reported and the oligomerization of Ste5 is essential for its ability to promote signaling. Self-interaction of Ste5 is thought to be mediated by a conformational switch associated with the activation of the signaling cascade[20, 21].

To address whether Ste5 is present as dimers or oligomers in the cytoplasm, we investigated the molecular brightness of the Ste5 particle by photon counting histograms[22] (see also Section 1.2.3.; data partially shown in Supplementary Fig. S3d). Additionally, we also constructed a strain that expressed simultaneously Ste5-3mGFP and Ste5-3mCherry. For both experiments, we found no indication for significant self-interaction of Ste5 in the cytoplasm, in either vegetative or pheromone-stimulated cells.

1.2.7. Quantification of the relative abundance of proteins at the shmoo tip

1.2.7.1 Description and validation of the method

By using confocal photon counting image analysis (see Methods), we measured the intensity of the fluorescent fusion proteins at the shmoo tip. The intensity that results due to protein present in the cytoplasmic volume in the region of interest was taken into account by subtracting the intensity of a corresponding volume measured in a cell peripheral region nearby. This yielded the fluorescence signal from the proteins specifically bound to the shmoo tip. Intensity values were calibrated in the cytoplasm by the population-average concentration measured by FCS.

This method, which allowed for the measurement of relative protein abundances at the shmoo tip, was validated by the obtained stoichiometry of approximately 1:1 for a Fus3 construct tagged with GFP at its N-terminus and with 3mCherry at its C-terminus (see Supplementary Information Fig. S5).

1.2.7.2. Additional discussion of the results

We observed a ratio of 1.7 molecules of Fus3 to 1 molecule of Ste5 in the shmoo tip bound fraction (Fig. 3a, b). It has to be noted that a fraction of the shmoo-tip-recruited Fus3 could be due to the bridging function of Ste7, which could in theory lead to a maximum ratio of Fus3:Ste5 = 2:1 in the shmoo tip. However, the observation of a 3-fold excess of Fus3 over Ste5 at the shmoo tip in the Msg5 down-regulation mutant (Fig. 4c) demonstrates that a fraction of Fus3 must be bound in a Ste5- and Ste7-independent way at the shmoo tip. This experiment also supports the notion that Fus3 recruitment to the shmoo tip occurs via substrate interactions, as the level of Fus3 recruitment correlates inversely with the amount of phosphatase present in the cells.

We furthermore noticed that wild type 3meGFP-tagged Fus3 exhibited a two-fold higher amount in the shmoo as compared to 3mCherry-tagged wild type Fus3, which may be caused by steric hindrance due to a shorter spacer sequence used to space the Fus3 coding sequence and 3mCherry as compared to the 3meGFP fusion (see Supplementary Information, section 1.1.2). For this reason, our value for the enrichment of Fus3 at the shmoo tip (Fig. 3b), which was obtained with the 3mCherry-tagged Fus3, is a conservative estimate.

Moreover, to investigate the bridging role of Ste7 directly we attempted to use binding-impaired Ste5 and Ste7 mutants, but these mutants failed to show membrane recruitment of Ste5 and shmoo formation. In particular, we investigated the

localization of Fus3 and Ste7 in the Ste5VASP mutant background, which is defective in binding to Ste7[20]. We found no shmoo formation and no membrane recruitment of Fus3 or Ste7 upon pheromone treatment. Additionally, we combined the Ste7ND1/2 mutant (impaired in Kss1 and Fus3 binding) with a Ste5ND mutant (specifically impaired in Fus3 binding but causing a hyper activation of the pathway upon stimulation[4]), to see whether there exists a compensatory effect of the two mutations. We found however that these cells do not shmoo. Furthermore, no membrane recruitment of either Fus3 or Ste7 was observed, probably due to impaired signaling. In conclusion, we could not use these two mutant strains to study the Ste5/Ste7 dependency of Fus3 recruitment to the shmoo tip.

1.2.8. Discussion of enzyme-substrate interactions of active $Fus3^{PP}$

A number of publications report that (i) substrates of active $Fus3^{PP}$ are present in the shmoo, and that (ii) $Fus3^{PP}$ is able to undergo relatively strong interactions with some of the substrates.

(i) Candidate substrates in the shmoo include Fus3 itself and the Ste5-bound machinery in feedback phosphorylation reactions, in particular Gpa1, which binds active $Fus3^{PP}$ directly[23]. Other substrates of Fus3 enriched in the shmoo include Far1[5, 24], which is bound via Bem1 to Ste5[25, 26], and Bni1, a formin protein involved in actin filament nucleation[27, 28].

(ii) ChIP-on-chip experiments with pheromone stimulated cells demonstrated Fus3 interactions with transcriptional regulators[29], suggesting that active $Fus3^{PP}$ is able to participate in relatively stable interactions with substrates.

1.2.9. Fluorescence lifetime imaging microscopy (FLIM)

1.2.9.1 Method for FLIM measurements

Sample preparation: Yeast cells were stimulated for 3 hours with 2 $\mu g \cdot ml^{-1}$ α-factor in liquid cultures. Cells were fixed by addition of 1 volume of 1 M $K_xH_yPO_4$, pH6.5 and 8% paraformaldehyde (freshly made) for 3 hours with occasional inversion. Cells were washed three times with SP buffer (0.1 M KPO_4, 1.2 M Sorbitol) and once with SP buffer containing 100 mM 3-Glycerophosphate (GP) and 20 mM β-Mercaptoethanol. The cell wall was removed by incubation with 1 $mg \cdot ml^{-1}$ Zymolase 100T (Seikagaku, Japan) at 30°C for 30–60 minutes in SP containing GP. Cells were washed four times with SP buffer containing GP and immobilized for 20 minutes on poly-L-lysine-coated multiwell glass-slides in a humid chamber. The wells on the slides were washed individually, once with PBS containing 0.1% TritonX-100, five times with PBS followed by incubation with PBS containing 1% bovine serum albumin (BSA Fraction V, Sigma) for 30 minutes. The slides were incubated overnight with Cy3-labeled antibodies at 4°C in a humid chamber. Thereafter, antibody solutions were replaced by fresh ones and the slides were sealed using a cover slip and nail polish. The slides were stored at 4°C for up to three days. Rabbit anti-GFP and anti-phospho-ERK1/ERK2 (anti-pTEpY) were Cy3-labeled and purified according to the protocol of the Cy3 labeling kit (GE Healthcare, Germany) resulting in labeling ratios of 2.9 and 5.1 of dye molecules per antibody respectively.

Image acquisition and analysis: FLIM images were obtained using a Fluoview 1000 microscope (Olympus, Germany) equipped with a Picoharp 300 photon counting setup (Picoquant, Germany). GFP was excited with a 470 nm diode (Sepia II, Picoquant, Germany) that was attenuated 10× by a neutral density filter. The excitation light was fiber-coupled into the confocal scan head and focused into the sample using a water immersion 60× UPlanSApo objective lens (N.A. 1.2). Emission

light passed a 405/470 dichroic mirror and a size-adjustable pinhole set to 1 Airy unit. The fluorescence was guided via a multimode fiber into the detection box containing a HQ500/40 emission filter and a single avalanche photon detector (SPAD, MPD, Italy). Images of 256×256 pixels were acquired during 4 minutes, corresponding to approximately 1 million detected photons. Images of the GFP (donor) fluorescence were processed using the SymPhoTime software package (v4.2, Picoquant, Germany). In order to estimate the fluorescence lifetime of GFP in yeast, fixed and permeabilized yeast cells expressing Fus3-GFP were measured in the absence of labeled antibody. Cells were masked and the time-correlated photon counting histograms were summed over multiple images. The fluorescence lifetime retrieved from this analysis was fixed in the experiments with the samples containing labeled antibodies, where two-exponential models have been used for data analysis. The second lifetime (corresponding to the population of GFP proteins which interacts with labeled antibody) was estimated by fitting the sum of the individual photon histograms over multiple images. This second lifetime was then fixed for fitting the individual images on a pixel-to-pixel basis. For quantification of the distribution of the lifetimes (Fig. 5c & d and Supplementary Information Fig. S6a-c), the resulting lifetime images were exported and analyzed in ImageJ. The GFP intensity image was used to generate a mask in order to outline the individual cells in the fluorescence lifetime image. The average lifetime values were superimposed on an axis of symmetry in the yeast cell, starting in the shmoo tip and ending at the distal end of the cell. The fluorescence lifetime images are presented in pseudo-color. For Fig. 5c, additionally the GFP intensity distribution was plotted by averaging the single-cell fluorescence distributions along the axis of symmetry (see above). These distributions were normalized to the highest and lowest intensity observed in the individual cell.

1.2.9.2. Additional discussion and controls for the FLIM experiment

The FLIM measurement investigates the interaction of endogenous level expressed Fus3-GFP (tagged at the C-terminus) and antibodies specific for phosphorylated MAP kinases. Although these Cy3-labeled antibody also binds well to phosphorylated Kss1 and one other phosphorylated MAP kinase (data not shown), only its specific interaction with GFP-labeled Fus3 is detected in the FLIM experiment through the reduction of the GFP fluorescence lifetime.

We noticed a globally-decreased fluorescence lifetime of GFP in unstimulated cells labeled with the pTEpY-Cy3 antibody (Fig. 5d, compare with Supplementary Information Fig. S6b and c), with values that were similar to the highest lifetimes observed in stimulated cells. This indicates a background due to low affinity binding of this (polyclonal) antibody to non-phosphorylated Fus3, as detected by Western blotting (Fig. 5e). Anti-GFP Cy3-labeled antibodies also showed a uniform decrease of the fluorescence lifetimes (Supplementary Information Fig. S6a), well below the lifetimes obtained when non-specific (Supplementary Information Fig. S6b) or no antibodies (Supplementary Information Fig. S6c) were used. This homogenous distribution of life times excludes a concentration artifact in our gradient measurement due to the local enrichment of GFP in the shmoo.

1.3. Computational modeling

1.3.1. Effective interaction strengths (K_D^{eff})

We define the effective interaction strength, K_D^{eff}, based on the dissociation constant, K_D, that would be expected for a purely binary interaction. Unlike K_D, which is simply a thermodynamic constant, K_D^{eff} can depend on the total concentrations of all interactors. This can be understood in terms of the simple model explained below of the effective binding interaction between differently labeled proteins A and B in the presence of an unlabeled protein C. There are three possibilities:
(1) *Neutral*: C does not affect the binding of B to A. The interaction between A and B is purely binary, with K_D^{eff} simply equal to the binary interaction constant K_D. (C might still bind A and/or B, but its binding does not affect the interaction of A and B and can therefore be neglected.)
(2) *Cooperative*: Bound C at A helps B to bind A (or vice versa). Here, the K_D^{eff} is a function of protein concentrations. (A and B might not even bind each other directly, but only through C.)
(3) *Competitive*: Bound C at A hinders B from binding A (or vice versa). Also, here, the K_D^{eff} is a function of protein concentrations.

(1) ***Neutral***

Here, we refer to a purely binary interaction between proteins A and B that is unaffected by the presence of any other proteins. We therefore need only to consider the three species A, B, and the complex AB. Our FCS results yield the total concentration of all complexes containing either A or B, which in this case is just

$$n_A^{FCS} = n_A^{\text{Total}} = n_A + n_{AB} \tag{6}$$
$$n_B^{FCS} = n_B^{\text{Total}} = n_B + n_{AB}, \tag{7}$$

where n_A and n_B are the concentrations of free A and B, and n_{AB} is the concentration of the complex AB. Similarly, our FCCS results generically yield the total concentration of all complexes containing both A and B, which in this case is just the complex AB

$$n_{AB}^{FCCS} = n_{AB}^{\text{Total}} = n_{AB}. \tag{8}$$

Here, the strength of the binding interaction given by detailed balance between A and B is simply

$$K_D = K_A^B = \frac{n_A n_B}{n_{AB}} = \frac{\left(n_A^{FCS} - n_{AB}^{FCCS}\right)\left(n_B^{FCS} - n_{AB}^{FCCS}\right)}{n_{AB}^{FCCS}}, \tag{9}$$

where $K_D = K_A^B$ is the binary dissociation constant.

(2)–(3) ***Cooperative/Competitive***

Here, the binding of C to A and/or B either enhances (cooperative) or inhibits (competitive) the interaction of A with B. We consider the simple case having the

following unique species: A, B, C, AB, AC, BC, and ABC. Complex formation is again dictated by detailed balance:

$$\begin{aligned} n_A n_B &= \mathrm{K}_A^B n_{AB} \\ n_B n_C &= \mathrm{K}_B^C n_{BC} \qquad n_{AB} n_C = \mathrm{K}_{AB}^C n_{ABC}, \\ n_A n_C &= \mathrm{K}_A^C n_{AC} \end{aligned} \tag{10}$$

which gives four independent interaction constants. Two other interaction constants can be expressed in terms of these four:

$$\mathrm{K}_{AC}^B = \frac{\mathrm{K}_A^B}{\mathrm{K}_A^C} \mathrm{K}_{AB}^C \tag{11}$$

$$\mathrm{K}_{BC}^A = \frac{\mathrm{K}_A^B}{\mathrm{K}_B^C} \mathrm{K}_{AB}^C. \tag{12}$$

The FCS-measured total concentrations of A and B will now contain contributions from four separate populations:

$$n_A^{\mathrm{FCS}} = n_A^{\mathrm{Total}} = n_A + n_{AC} + n_{AB} + n_{ABC} \tag{13}$$

$$n_B^{\mathrm{FCS}} = n_B^{\mathrm{Total}} = n_B + n_{BC} + n_{AB} + n_{ABC}. \tag{14}$$

Similarly, the observed FCCS concentration of complex AB will be comprised of two populations:

$$n_{AB}^{FCCS} = n_{AB}^{\mathrm{Total}} = n_{AB} + n_{ABC}. \tag{15}$$

The effective binding interaction constant, $\mathrm{K}_{\mathrm{D}}^{\mathrm{eff}}$, is defined just as above for the purely binary interaction in terms of the FCS and FCCS results:

$$\mathrm{K}_{\mathrm{D}}^{\mathrm{eff}} \equiv \frac{\left(n_A^{FCS} - n_{AB}^{FCCS}\right)\left(n_B^{FCS} - n_{AB}^{FCCS}\right)}{n_{AB}^{FCCS}} = \frac{\left(n_A + n_{AC}\right)\left(n_B + n_{BC}\right)}{n_{AB} + n_{ABC}} = \mathrm{K}_A^B \frac{\left(1 + \frac{n_C}{K_A^C}\right)\left(1 + \frac{n_C}{K_B^C}\right)}{1 + \frac{n_C}{K_{AB}^C}}. \tag{16}$$

$\mathrm{K}_{\mathrm{D}}^{\mathrm{eff}}$ depends on the various interaction constants, but also on the unknown concentration of free C, which itself is a function of the interaction constants and the total concentrations of each interactor. The relative strengths of the various interactions can generate either cooperative or competitive roles for protein C. In the absence of protein C ($n_C = 0$), $\mathrm{K}_{\mathrm{D}}^{\mathrm{eff}}$ is simply equal to the binary interaction constant K_A^B. This model can be straighforwardly extended to the case of multiple unknown interactors (proteins C, D, E, F, ...).

Despite the concentration-dependence of $\mathrm{K}_{\mathrm{D}}^{\mathrm{eff}}$, it is still valid to compare $\mathrm{K}_{\mathrm{D}}^{\mathrm{eff}}$ calculated for two populations of cells with similar component concentrations, as we do for unstimulated and stimulated cells in Fig. 2. Importantly, the stimulated cells were observed within the first hour of stimulation to avoid changes in overall protein concentration levels.

1.3.1. Reaction-diffusion model of active Fus3 gradient

The following 1D reaction-diffusion equations are proposed to describe Fus3 binding/unbinding and phosphorylation at the shmoo tip, as well as its dephosphorylation in the cytoplasm:

$$\frac{\partial F(x,t)}{\partial t} = D\nabla^2 F(x,t) + pF_p(x,t) - b_{on}B(x)\,F(x,t) + b_{off}C(x,t) \quad (17)$$

$$\frac{\partial F_p(x,t)}{\partial t} = D\nabla^2 F_p(x,t) - pF_p(x,t) - b_{on}B(x)\,F_p(x,t) + b_{off}C_p(x,t) \quad (18)$$

$$\frac{\partial C(x,t)}{\partial t} = -k\,C(x,t) + pC_p(x,t) - b_{off}C(x,t) + b_{on}B(x)\,F(x,t) \quad (19)$$

$$\frac{\partial C_p(x,t)}{\partial t} = k\,C(x,t) - pC_p(x,t) - b_{off}C_p(x,t) + b_{on}B(x)\,F_p(x,t), \quad (20)$$

with $F(x,t)$ and $F_p(x,t)$, the freely-diffusing unphosphorylated and phosphorylated Fus3 concentrations; D, the Fus3 diffusion constant; b_{on} and b_{off}, the binding on and off rates at the shmoo tip; $B(x)$, the concentration (per volume of the cytoplasm) of free binding sites for both unphosphorylated and phosphorylated Fus3 at the shmoo tip; $C(x,t)$ and $C_p(x,t)$, the concentrations (per volume of the cytoplasm) of unphosphorylated and phosphorylated Fus3 bound at the shmoo tip; $k = \frac{k_{cat}^K}{M_K} f K \frac{V}{A\,dl}$, the phosphorylation rate due to kinases bound at the shmoo tip with k_{cat}^K the catalytic rate constant, M_K the Michaelis-Menten constant, f the fraction of kinase bound at the shmoo tip, K the total concentration of kinase (per volume of the cytoplasm), V the cytoplasm volume, A the shmoo surface area, and dl a measure of the effective change in the 3D catalytic parameters due to the reduction of dimension (and other changes) in the 2D membrane; and $p = \sum_i \frac{k_{cat}^{P_i}}{M_{P_i}} P_i$, the total cytoplasmic dephosphorylation rate due to multiple phosphatases with $k_{cat}^{P_i}$ the catalytic rate constant, M_{P_i} the Michaelis-Menten constant, and P_i the cytoplasmic concentration of the *i*th phosphatase. All enzymes are assumed to be unsaturated (this has been confirmed using FCCS in the case of Msg5 and Fus3 by the absence of significant cross-correlation, not shown). A simple 1D geometry is taken, with the cell extending from $x = 0$ (shmoo tip) to $x = L$ (distal end). For simplicity, we assume that binding/unbinding and phosphorylation at the shmoo tip are separate processes. For phosphorylation, $F_p(x)$ corresponds to doubly-phosphorylated Fus3 (a single interaction of unphosphorylated Fus3 with kinase results in double-phosphorylation and phosphorylated Fus3 with phosphatase results in double-dephosphorylation). More complicated models could be assumed (e.g., where binding at the shmoo tip is dependent on phosphorylation or where singly-phosphorylated Fus3 is tracked), but they would all result in a gradient of active Fus3, since such a gradient is only dependent on the spatial partitioning of shmoo-tip kinases and cytoplasmic phosphatases of Fus3 with the contrast of the gradient determined solely by the diffusion constant of Fus3 (D) and the cytoplasmic dephosphorylation rate (p).

In steady-state,

$$C(x) = \frac{b_{on}B(x)}{b_{off}} \frac{(p + b_{off})F(x) + pF_p(x)}{k + p + b_{off}} \tag{21}$$

$$C_p(x) = \frac{b_{on}B(x)}{b_{off}} \frac{kF(x) + (k + b_{off})F_p(x)}{k + p + b_{off}}, \tag{22}$$

giving

$$0 = D\nabla^2 F(x) + pF_p(x) + b_{on}B(x) \frac{-kF(x) + pF_p(x)}{k + p + b_{off}} \tag{23}$$

$$0 = D\nabla^2 F_p(x) - pF_p(x) + b_{on}B(x) \frac{kF(x) - pF_p(x)}{k + p + b_{off}}. \tag{24}$$

Adding these two equations gives $\nabla^2\left(F(x) + F_p(x)\right) = 0$, with solution $F(x) + F_p(x) = F_{cyt}$. We therefore need only solve for the phosphorylated Fus3 distribution, $F_p(x)$. Binding and phosphorylation at the shmoo tip can be taken into account as boundary conditions (see below). We can then write the phosphorylated substrate steady-state equations for each region as:

$$0 = D\nabla^2 F_p^c(x) - p\,F_p^c(x), \tag{25}$$

which is now only in terms of the unphosphorylated substrate and has following general solution:

$$F_p^c(x) = G\mathrm{e}^{\kappa x} + H\mathrm{e}^{-\kappa x}, \tag{26}$$

where $\kappa = \sqrt{p/D}$. The hard-wall (Neumann) boundary condition at $x = L$ gives a zero-slope boundary condition there:

$$\left.\frac{dF_p}{dx}\right|_{x=L} = G\kappa\mathrm{e}^{\kappa L} - H\kappa\mathrm{e}^{-\kappa L} = 0, \tag{27}$$

or

$$F_p = I\cosh\kappa(L - x). \tag{28}$$

The boundary condition at the shmoo tip can be obtained from "Gauss's Law" applied to Eq. 13, taking $B(x) = \frac{BV}{A}\delta(x) = BL\delta(x)$, where B is the concentration (per cytoplasmic volume) of free binding sites and $\delta(x)$ is a δ-function at the shmoo tip:

$$\left.\frac{dF_p}{dx}\right|_{x=0} = -\frac{b_{on}BL}{D} \frac{k\left(F_{cyt} - F_p(0)\right) - pF_p(0)}{k + p + b_{off}} \tag{29}$$

$$-I\kappa\sinh\kappa L = -\frac{b_{on}BL}{D} \frac{kF_{cyt} - (k + p)I\cosh\kappa L}{k + p + b_{off}}, \tag{30}$$

giving the following solution for I:

$$I = \frac{1}{\cosh \kappa L + \left(1 + \frac{b_{off}}{k+p}\right)\frac{D\kappa}{b_{on}BL}\sinh \kappa L}\,\frac{k}{k+p}F_{cyt}. \qquad (31)$$

Plugging in for $\kappa = \sqrt{p/D}$, the phosphorylated Fus3 distribution is then:

$$F_p(x) = \frac{1}{\cosh\sqrt{\frac{p}{D}}L + \left(1 + \frac{b_{off}}{k+p}\right)\frac{\sqrt{pD}}{b_{off}L}\frac{b_{off}}{b_{on}B}\sinh\sqrt{\frac{p}{D}}L}\,\frac{k}{k+p}F_{cyt}\cosh\sqrt{\frac{p}{D}}(L-x), \qquad (32)$$

with unphosphorylated distribution simply $F(x) = F_{cyt} - F_p(x)$.

The relative amount of Fus3 bound at the shmoo tip compared with Fus3 freely-diffusing in the cytoplasm is just:

$$\frac{\int (C(x) + C_p(x))\,dV}{\int F_{cyt}dV} = \int \frac{b_{on}B(x)}{b_{off}}F_{cyt}\,dV \Big/ \int F_{cyt}dV = \int \frac{b_{on}B\frac{V}{A}}{b_{off}}\delta(x-b)F_{cyt}dV \Big/ \int F_{cyt}dV = \frac{b_{on}B}{b_{off}}. \qquad (33)$$

This ratio is equal to the ratio of the integrated image intensities in the shmoo tip and the cytosol:

$$\frac{b_{on}B}{b_{off}} = \frac{\int_{shmoo} I\,dV}{\int_{cytosol} I\,dV}, \qquad (34)$$

which we find to be roughly 0.02 from quantitative imaging, implying about 2% of cytosolic Fus3 is bound at the shmoo tip.

The parameters we used for the simulation in Fig. 5b were as follows:

<u>Measured:</u>	
$D = 4.2\ \mu m^2 \cdot s^{-1}$	Diffusion constant of Fus3, as determined by FCS
$L = 8\ \mu m$	Length of a cell with a shmoo
$\frac{b_{on}B}{b_{off}} = 0.02$	Measured from image; see explanation to (33)
$b_{off} = 2\ s^{-1}$	From FRAP Fus3 recovery at shmoo tip ($b_{off} \geq 2\ s^{-1}$, see Fig. 4c in van Drogen et al[30])
<u>Assumed:</u>	
$p = 1\ s^{-1}$	Phosphatase rate; see Fig. 5a and explanation in the main text.

$k = 10\ s^{-1}$	Kinase rate; to generate a high fraction of phosphorylated Fus3 at the shmoo tip, k must be a factor of a few greater than p.

Supplementary Figures S1 to S6

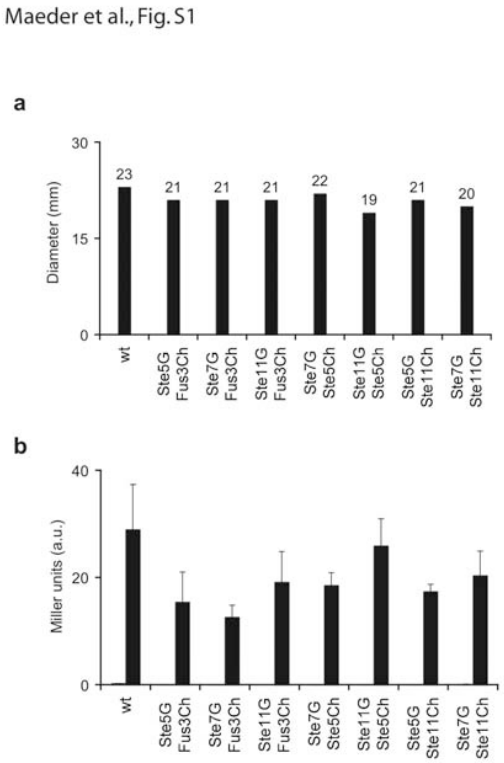

Figure S1 Expression of fluorescent protein tagged proteins does not interfere with pheromone signaling. (**a**) Halo assays were used to assess the cell cycle arrest response of the used strains upon pheromone stimulation. The diameter of the growth-inhibited zone around a pheromone source is comparable in wild type and fluorescent protein expressing strains. (**b**) Expression of a LacZ reporter under control of a pheromone responsive promoter (P_{FUS1}) was assayed following 90 min of pheromone stimulation.

Maeder et al., Supplementary Information Fig. S2

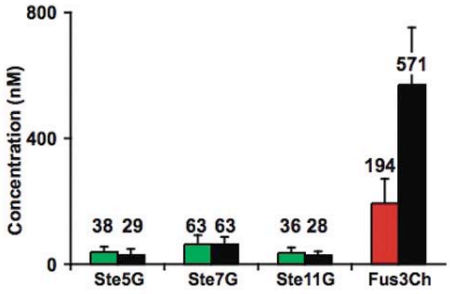

Figure S2 Concentration of Ste5, Ste7, Ste11 and Fus3 in the cytoplasm of vegetative (colored bars, red for 3mCherry constructs, green for 3meGFP constructs) and α-factor stimulated (black) yeast cells (2.5-3 hours after addition of pheromone), measured using FCS.

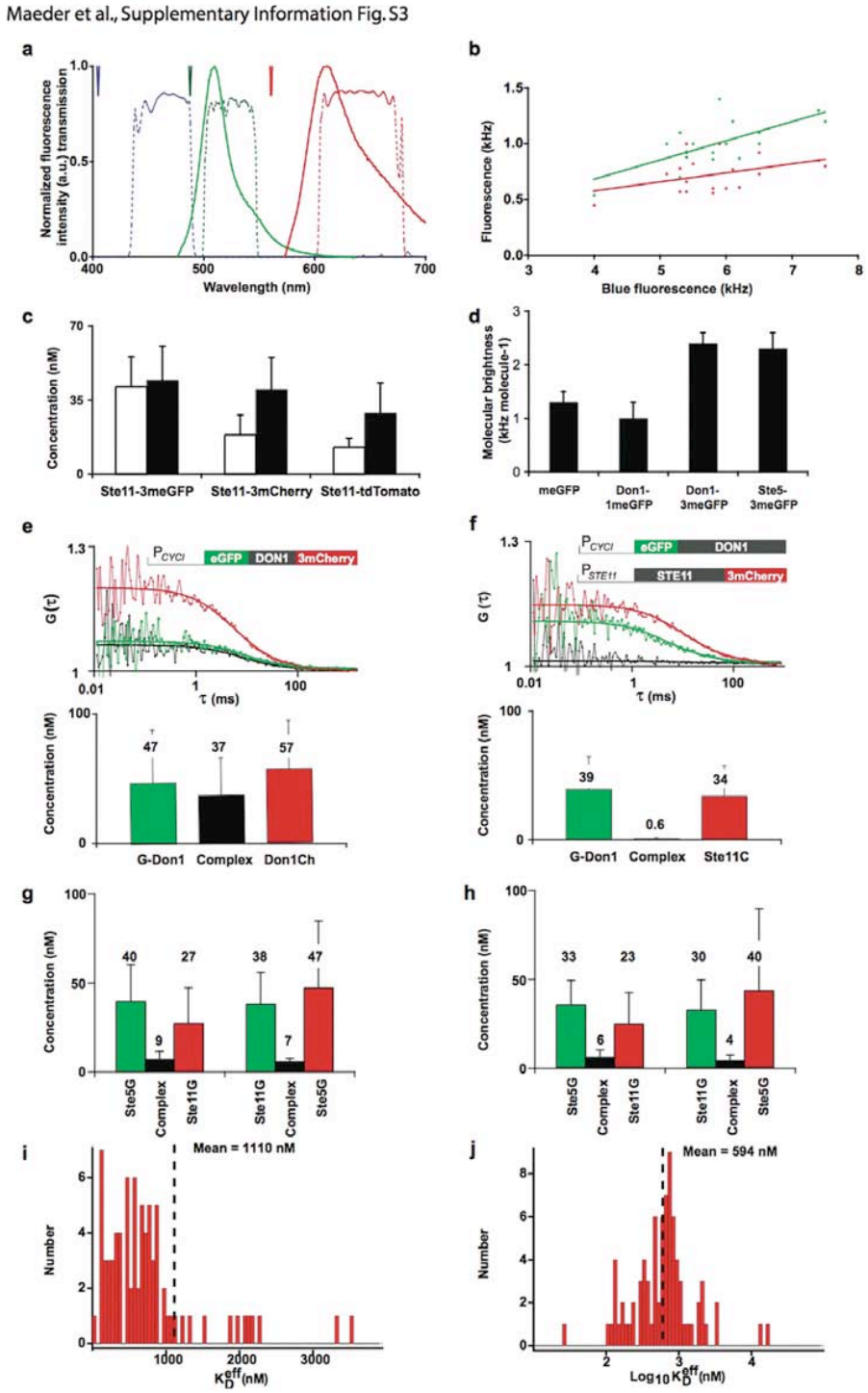

Figure S3 Setup and validation of the FCCS method. (**a**) FCCS setup: Filter sets used for FCCS measurements (red and green dashed lines) and for estimation of the autofluorescence (blue dashed line). Continuous lines represent eGFP (green) and mCherry (red) emission spectra. Arrows from the top indicate the laser lines used for excitation. (**b**) Correlation of wild type yeast autofluorescence between the different detection channels (blue vs. green and red) (see Section 1.2.3). (**c**) Fluorescent protein maturation. Yeast cells expressing Ste11 fused to 3meGFP, 3mCherry or tdTomato

were incubated in SC medium with (black) or without (white) cycloheximide for 3 hours in order to block protein synthesis and to allow complete maturation of the fluorescent proteins. Mean values and standard deviations of the concentrations, as determined by FCS, are displayed for each eight cell measurements. (**d**) Molecular brightness analysis by photon counting histogram of yeast cells expressing free meGFP, Don1 fusions to single and triple copies of meGFP or Ste5-3meGFP. Please note the same molecular brightness of Don1 and Ste5 fused to 3meGFP indicating that Ste5[31], similar to Don1 is present as a monomer in the cytoplasm of vegetative cells. **(e)**, **(f)** Validation of FCCS measurements in yeast using control constructs (**e**) Auto- (green and red) and cross-correlation (black) curves of cells expressing eGFP and 3mCherry fused to both ends of the spacer protein Don1 (positive control). The cartoon depicts the used constructs. (**f**) Negative control, cells expressing eGFP-Don1 and Ste11-3mCherry. Total concentration of the fusion proteins and the common complexes are given below the corresponding FCCS curves. Mean values and standard deviations of single-cell measurements (e, n=37 cells; f, n=23 cells) were not corrected for non-perfect overlap of the detection volumes. (**g**), (**h**) FCS/FCCS measurements are independent on the specific fluorescent protein used for gene fusion. FCCS analysis of yeast cells expressing Ste5 and Ste11 tagged with 3meGFP and 3mCherry or vice versa. Quantification of complexes in (**g**) vegetative and (**h**) α-factor stimulated yeast cells (g & h, n=20 cells). (**i**) Calculation of the mean K_D^{eff} for the Ste11-Fus3 interaction in pheromone stimulated cells using normal or (**j**) log-normal units (same data set as shown in Fig. 2). Transformation of the histogram for all measurements into log space yields a normal distribution of the measurements, which then can be used to calculate the mean and the standard deviations (for further explanations, see the Methods section in the main manuscript).

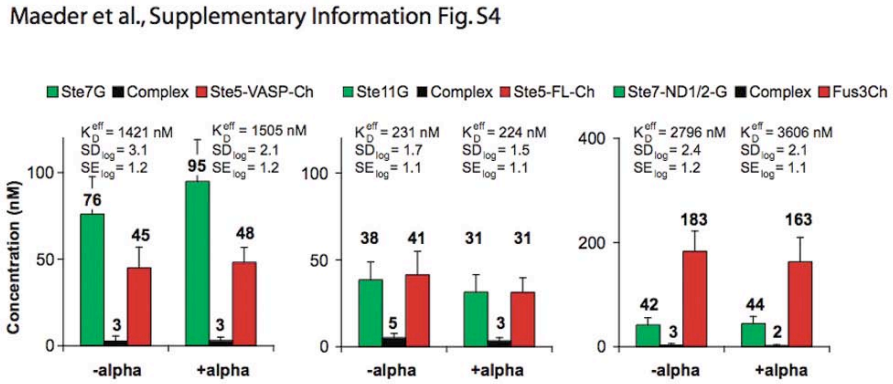

Figure S4 Interaction mutants validate the specificity and the sensitivity of the FCCS measurements. Decreased protein complex concentration and increased K_D^{eff} values were obtained in binding-impaired mutants. The following mutants and interactions were investigated: $Ste5^{VASP}$ (Ste5 with V763A, S861P)[20] interaction with Ste7, $Ste5^{FL}$ (Ste5 with F5141L)[20] interaction with Ste11; $Ste7^{ND1/2}$ (Ste7 with R9A,R10A,L15A,L17A, R62A,R63A,L69A,L71A)[5] interaction with Fus3. The significantly higher K_D^{eff} values, as compared with the wild type interactions (Fig. 2), confirm that these mutants are impaired in the specific interaction.

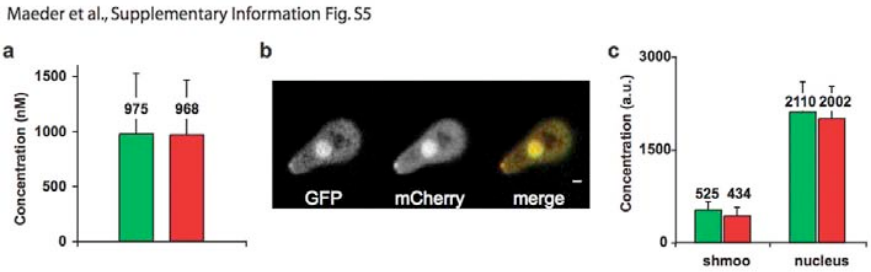

Figure S5 Proof of principle for the quantitative measurement of protein abundance in the shmoo using FCS data for the calibration of quantitative APD imaging. (**a**) Protein concentration of eGFP-Fus3-3mCherry (expressed from the P_{ADH}-promoter) in the cytoplasm of stimulated cells (2.5 - 3 hours pheromone stimulation) measured by FCS. Means of the measurements (n = 24 cells) and standard deviations are shown. (**b**) APD images of stimulated eGFP-Fus3-3mCherry cells. Bar corresponds to 1 μm. (**c**) Enrichment of GFP versus Cherry in the shmoo and the nucleus determined using quantification of the APD images. Means of the measurements (n = 13 cells) and standard errors are shown. (a.u., arbitrary units)

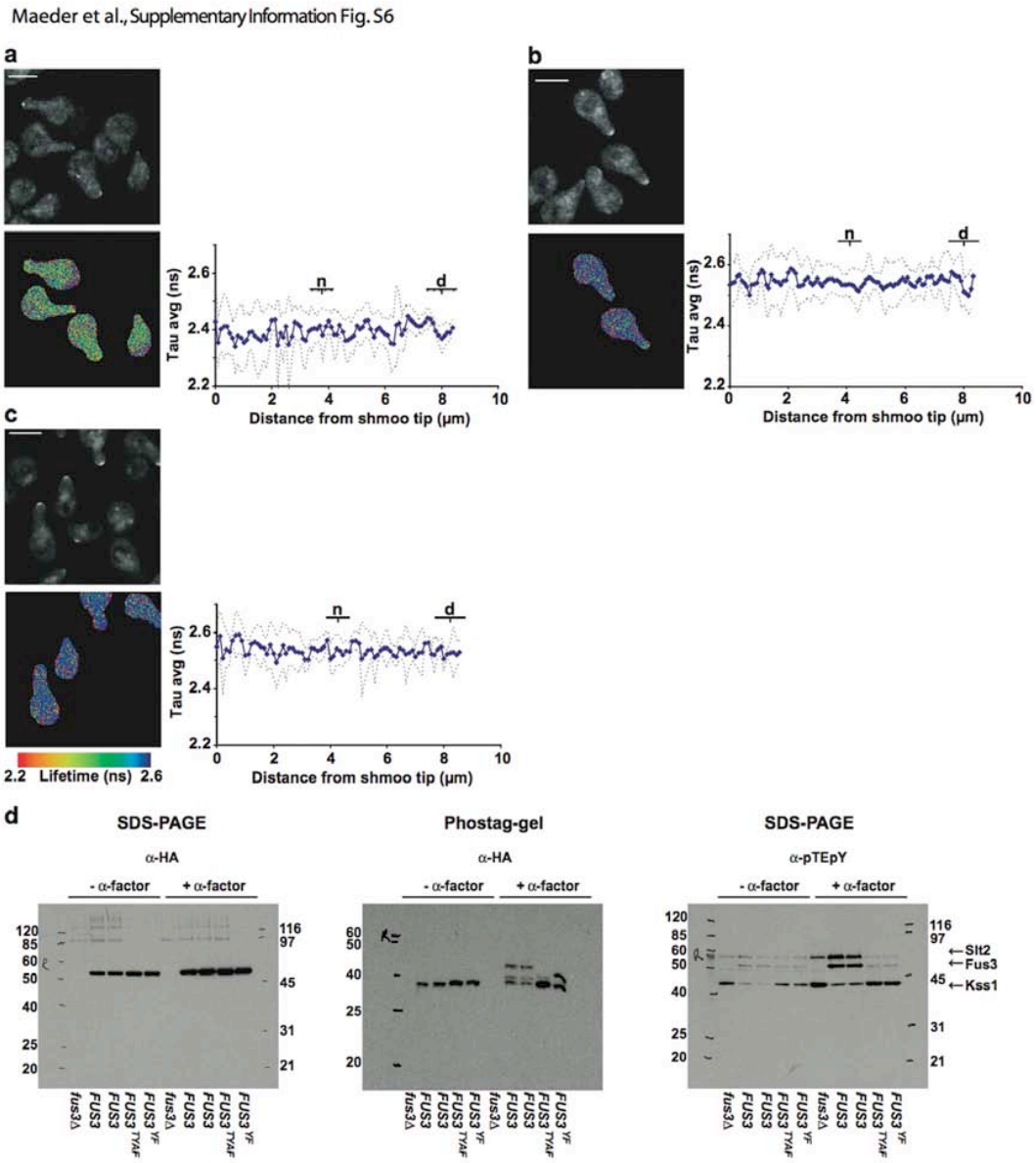

Figure S6 The FLIM experiment specifically detects active Fus3^{PP}. Additional controls are shown to validate the specificity of detection. Experiments using the following Cy3-labeled antibodies are shown: (**a**) anti-GFP (n=25 cells), (**b**) anti-Rabbit (n=30 cells) and (**c**) no antibody (n=28 cells). Experimental details and the format of data presentation are as described in legend to Figure 5 in the main manuscript. Details about the method are presented in section 1.2.9.1**,** a discussion of the controls is provided in section 1.2.9.2. (**d**) Full scans of the Western blots shown in Fig. 5e of the main manuscript. The antibody specific to anti-phospho ERK1/2 (anti-pTEpY) recognizes weakly the non-phosphorylated Fus3 and in addition phosphorylated Kss1[32] and one other MAP kinase (probably Slt2[33]). For the assignment of molecular weight markers, please note that phostag-gel electrophoresis, while allowing the separation of different phosphorylated forms of a protein, also affects the mobility of polypeptides in a non-predictable way. Hence, the positions of the molecular weight markers cannot be used to identify a protein. This has to be achieved by normal SDS-PAGE gel electrophoresis and additional controls, such as the use of deletion strains. These controls are included in the figure.

3. References

1. Guthrie, C. & Fink, G.R. Guide to Yeast Genetics and Molecular Biology. *Meth Enzymol* **194**, 429 and 663 (1991).
2. Janke, C. *et al.* A versatile toolbox for PCR-based tagging of yeast genes: new fluorescent proteins, more markers and promoter substitution cassettes. *Yeast* **21**, 947-962 (2004).
3. Taxis, C. & Knop, M. System of centromeric, episomal, and integrative vectors based on drug resistance markers for Saccharomyces cerevisiae. *Biotechniques* **40**, 73-78 (2006).
4. Bhattacharyya, R.P. *et al.* The Ste5 scaffold allosterically modulates signaling output of the yeast mating pathway. *Science* **311**, 822-826 (2006).
5. Remenyi, A., Good, M.C., Bhattacharyya, R.P. & Lim, W.A. The role of docking interactions in mediating signaling input, output, and discrimination in the yeast MAPK network. *Mol Cell* **20**, 951-962 (2005).
6. Shaner, N.C. *et al.* Improved monomeric red, orange and yellow fluorescent proteins derived from Discosoma sp. red fluorescent protein. *Nat Biotechnol* **22**, 1567-1572 (2004).
7. Cormack, B.P. *et al.* Yeast-enhanced green fluorescent protein (yEGFP)a reporter of gene expression in Candida albicans. *Microbiology* **143 (Pt 2)**, 303-311 (1997).
8. Chalfie, M., Tu, Y., Euskirchen, G., Ward, W.W. & Prasher, D.C. Green fluorescent protein as a marker for gene expression. *Science* **263**, 802-805 (1994).
9. Knop, M. *et al.* Epitope tagging of yeast genes using a PCR-based strategy: more tags and improved practical routines. *Yeast* **15**, 963-972 (1999).
10. Kinoshita, E., Kinoshita-Kikuta, E., Takiyama, K. & Koike, T. Phosphate-binding tag, a new tool to visualize phosphorylated proteins. *Mol Cell Proteomics* **5**, 749-757 (2006).
11. Valtz, N. & Peter, M. Functional analysis of FAR1 in yeast. *Methods Enzymol* **283**, 350-365 (1997).
12. Pereira, G., Tanaka, T.U., Nasmyth, K. & Schiebel, E. Modes of spindle pole body inheritance and segregation of the Bfa1p-Bub2p checkpoint protein complex. *Embo J* **20**, 6359-6370 (2001).
13. Strickfaden, S.C. *et al.* A mechanism for cell-cycle regulation of MAP kinase signaling in a yeast differentiation pathway. *Cell* **128**, 519-531 (2007).
14. Eid, J.S., Muller, J.D. & Gratton, E. Data acquisition card for fluctuation correlation spectroscopy allowing full access to the detected photon sequence. *Review of Scientific Instruments* **71**, 361-368 (2000).
15. Skakun, V.V. *et al.* Global analysis of fluorescence fluctuation data. *Eur Biophys J* **34**, 323-334 (2005).
16. Haupts, U., Maiti, S., Schwille, P. & Webb, W.W. Dynamics of fluorescence fluctuations in green fluorescent protein observed by fluorescence correlation spectroscopy. *Proceedings of the National Academy of Sciences of the United States of America* **95**, 13573-13578 (1998).
17. Delon, A., Usson, Y., Derouard, J., Biben, T. & Souchier, C. Photobleaching, mobility, and compartmentalisation: inferences in fluorescence correlation spectroscopy. *J Fluoresc* **14**, 255-267 (2004).

18. Chen, Y., Muller, J.D., So, P.T. & Gratton, E. The photon counting histogram in fluorescence fluctuation spectroscopy. *Biophys J* **77**, 553-567 (1999).
19. Muller, J.D. Cumulant analysis in fluorescence fluctuation spectroscopy. *Biophys J* **86**, 3981-3992 (2004).
20. Inouye, C., Dhillon, N., Durfee, T., Zambryski, P.C. & Thorner, J. Mutational analysis of STE5 in the yeast Saccharomyces cerevisiae: application of a differential interaction trap assay for examining protein-protein interactions. *Genetics* **147**, 479-492 (1997).
21. Inouye, C., Dhillon, N. & Thorner, J. Ste5 RING-H2 domain: role in Ste4-promoted oligomerization for yeast pheromone signaling. *Science* **278**, 103-106 (1997).
22. Chen, Y., Wei, L.N. & Muller, J.D. Unraveling protein-protein interactions in living cells with fluorescence fluctuation brightness analysis. *Biophys J* **88**, 4366-4377 (2005).
23. Metodiev, M.V., Matheos, D., Rose, M.D. & Stone, D.E. Regulation of MAPK function by direct interaction with the mating-specific Galpha in yeast. *Science* **296**, 1483-1486 (2002).
24. Elion, E.A., Satterberg, B. & Kranz, J.E. FUS3 phosphorylates multiple components of the mating signal transduction cascade: evidence for STE12 and FAR1. *Mol Biol Cell* **4**, 495-510 (1993).
25. Leeuw, T. *et al.* Pheromone response in yeast: association of Bem1p with proteins of the MAP kinase cascade and actin. *Science* **270**, 1210-1213 (1995).
26. Lyons, D.M., Mahanty, S.K., Choi, K.Y., Manandhar, M. & Elion, E.A. The SH3-domain protein Bem1 coordinates mitogen-activated protein kinase cascade activation with cell cycle control in Saccharomyces cerevisiae. *Mol Cell Biol* **16**, 4095-4106 (1996).
27. Matheos, D., Metodiev, M., Muller, E., Stone, D. & Rose, M.D. Pheromone-induced polarization is dependent on the Fus3p MAPK acting through the formin Bni1p. *J Cell Biol* **165**, 99-109 (2004).
28. Qi, M. & Elion, E.A. Formin-induced actin cables are required for polarized recruitment of the Ste5 scaffold and high level activation of MAPK Fus3. *J Cell Sci* **118**, 2837-2848 (2005).
29. Pokholok, D.K., Zeitlinger, J., Hannett, N.M., Reynolds, D.B. & Young, R.A. Activated signal transduction kinases frequently occupy target genes. *Science* **313**, 533-536 (2006).
30. van Drogen, F., Stucke, V.M., Jorritsma, G. & Peter, M. MAP kinase dynamics in response to pheromones in budding yeast. *Nat Cell Biol* **3**, 1051-1059 (2001).
31. Elion, E.A. The Ste5p scaffold. *J Cell Sci* **114**, 3967-3978 (2001).
32. Sabbagh, W., Jr., Flatauer, L.J., Bardwell, A.J. & Bardwell, L. Specificity of MAP kinase signaling in yeast differentiation involves transient versus sustained MAPK activation. *Mol Cell* **8**, 683-691 (2001).
33. Zarzov, P., Mazzoni, C. & Mann, C. The SLT2(MPK1) MAP kinase is activated during periods of polarized cell growth in yeast. *Embo J* **15**, 83-91 (1996).